

PARTIAL DISCHARGE DETECTION IN MEDIUM VOLTAGE STATORS USING TWO
INDEPENDENT DETECTION SCHEMES

By

Akshay Bhure

A THESIS

Submitted to
Michigan State University
in partial fulfillment of the requirements
for the degree of

Electrical Engineering-Master of Science

2017

ABSTRACT

PARTIAL DISCHARGE DETECTION IN MEDIUM VOLTAGE STATORS USING TWO INDEPENDENT DETECTION SCHEMES

By

Akshay Bhure

With the increasing concerns over the breakdown of insulation in electrical machines, development of a standard test procedure for insulation testing has gained importance. One of the dominant effects that contribute towards insulation breakdown is Partial Discharges (PD). In this work, an attempt is made to come up with an accurate, reliable and repeatable procedure to test medium voltage stators for PD.

Partial Discharges (PD), once initiated, give rise to progressive deterioration of insulation material and lower its life expectancy. If allowed to persist, PD can even lead to the electric breakdown of insulation.

A PD detection technique developed for medium voltage stator insulation by utilizing two independent detection schemes is presented here. This PD detection technique aims to facilitate the testing of these stators at the end of their production and not their predictive maintenance. An IRIS PDA-IV filter was used along with an antenna to record PD events produced inside the stator insulation of medium voltage AC machines. To reduce the effect of noise on detections, some grounding techniques were incorporated and later a discrete time wavelet transform was used to de-noise both filter and antenna output. To extract the best out of the technique, both signals were analyzed together on a repetitive basis to make a confident decision after their correlation. In addition, an attempt was made through Linear Discriminant Analysis to classify the test samples based on some features of the signal.

Copyright by
AKSHAY BHURE
2017

ACKNOWLEDGEMENTS

I would begin by expressing my sincere gratitude to my advisor Dr. Elias G. Strangas for his continuous guidance and support throughout my journey as a graduate student at Michigan State University. His door was always open to me for useful talks, discussions, ideas on required topics, which always provided right direction to my research and writing work.

In addition, I would like to thank Dr. Edward Rothwell and Dr. Shanelle Foster for their precious time and willingness to be members of my graduate committee. I cannot proceed without mentioning the help and advice I received from Professor Rothwell on the work related to antennas.

Moreover, this work was not possible without the resources and help I received from Electric Motors and Drives Laboratory (EMDL). I am very thankful to Dr. Shanelle Foster for her invaluable views and suggestions. I was fortunate to share the Lab space with amazing talents like Cristian A. Lopez-Martinez, Abdullah Alfehaid, Will Jensen, Thang Pham, Reemon Haddad and Rodney Singleton, since I started. Their involvement and support as a team were priceless, which always encouraged me to achieve my goals. In the meantime, I also made great friends like Heinrich T. Eickhoff, Matt Meier, John Nachazel, Valbona Vulaja and Shaopo Huang. A unique thing I really liked about the lab was that it involved people from different cultural backgrounds, which reflected its diversity and strength as a group. I cannot forget the fun I had while working together late in the lab, the key insights from group meetings, laughter and jokes shared in the office, and much more. I will cherish these stories and moments from EMDL throughout my life.

I would also like to acknowledge the R&D team at General Motors John Agapiou, Ron Lesperance and Ryan Doherty with whom I collaborated with on the project. I appreciate their time and interest to provide me a platform, to work on the new ideas.

I will always be grateful to my family: My parents Dhananjay Bhure and Mala Bhure who

always showered their love and blessings on me, my soul mate Ketki Bhure who was always by my side in my toughest times I faced. It was their belief in me, which kept me motivated emotionally and mentally to keep achieving my dreams. I consider myself lucky to spend my childhood with my grandparents: Late Madhukar Rao Bhure, Sulochana Bhure, Anand Rao Patil and Late Anjira Patil, who always nurtured me to become a successful person.

TABLE OF CONTENTS

LIST OF FIGURES	vii
I. INTRODUCTION	1
II. BACKGROUND	2
2.1 Partial Discharge	2
2.2 Wavelet Transform	6
2.3 Linear Discriminant Analysis	10
2.4 Hilbert Transform and Envelope Detection.....	13
III. WORK PERFORMED	14
3.1 Experimental Setup	15
3.2 Signal Conditioning In LabVIEW	18
3.2.1. <i>Extraction of Partial Discharge signal</i>	18
3.2.2. <i>Second Level Denoising process</i>	20
IV. EXPERIMENTAL PROCEDURE	22
V. EXPERIMENTAL RESULTS	25
VI. CONCLUSIONS AND FUTURE WORK	34
APPENDIX	35
REFERENCES	42

LIST OF FIGURES

Figure 1: Impedance diagram of PD test setups, which use voltage measurements techniques	4
Figure 2: Wavelet function for Daubechies 14(db14) (a) and Daubechies 4(db4) (b).....	7
Figure 3: Scaling and shifting process during decomposition of signal using UWT.....	7
Figure 4: Scaling/dilation process for UWT, explained by filter bank algorithm	8
Figure 5: Signal Reconstruction using inverse- UWT, explained by filter bank algorithm	9
Figure 6: Linear Discriminant Analysis to maximize separability between two classes.....	10
Figure 7: Laboratory setup for PD detection using filter at stator ends.....	15
Figure 8: Grounded steel plate setup block diagram for reliable PD detection using filter and an antenna simultaneously	16
Figure 9: Grounded steel plate actual setup for reliable PD detection using filter and an antenna simultaneously.....	17
Figure 10: PD test response from filter (A), antenna (B) for applied impulse of 2.25KV (C) from test setup shown in figure 2 and 3.....	18
Figure 11: Raw PD response on antenna (A) and extracted PD signal from antenna (B).....	19
Figure 12: Comparison between PD response of filter before denoising (A) and after denoising (B).....	20
Figure 13: Noisy peak in DWT treated antenna output	21
Figure 14: Flow Chart showing Signal Reconditioning process in LabVIEW.....	22
Figure 15: Threshold reference levels for filter (A) and antenna (B) outputs	23
Figure 16: Envelope extraction of filter (A) and antenna (B) outputs.....	24
Figure 17: Overall agreement comparison and PD agreement comparison and correction logic.....	25
Figure 18: Comparison of PD detection in antenna and filter, with and without grounded steel plate for stator X26RA-175	27

Figure 19: PD Inception voltages for stator X26RB-1_UV (10 trials).....	28
Figure 20: PD Inception voltages for stator X26RB-1_UV with repeatability	29
Figure 21: PD Inception voltages before and after eliminating noise by checking peak durations for stator X26RB-126 (20 trials).....	30
Figure 22: PD Inception voltages before and after eliminating noise by checking peak durations for stator X26RA-175 (20 trials).....	31
Figure 23: 2D representation of 4D sample dataset using LDA, showing maximum separability between classes.	32
Figure 24: Programing blocks in LabVIEW which represent test data file (.csv) being read, rows of headers being separated and then matrix size is determined for setting the loop structures	36
Figure 25: Process followed to decompose antenna signal by using “WA Undecimated Wavelet Transform VI” with settings of dB 6 and level 6. This provided wavelet decomposition level 4 scale which was used to detect PD events by the antenna.....	36
Figure 26: Process followed to decompose filter signal by using “WA Undecimated Wavelet Transform VI” with settings of dB 14 and level 10. Levels 8 and 9 were selected for reconstruction through “WA Inverse Undecimated Wavelet Transform VI”. This provided reconstructed filter output, which was used to detect PD events by the filter	37
Figure 27: The values at the first and last 25 samples of denoised antenna output were set to zero to treat the end-condition problem in antenna waveform	37
Figure 28: Envelopes of the denoised antenna and filter outputs are found and then cross-correlation coefficient is calculated using both to reflect similarity between the two signals	38
Figure 29: Peak to Peak values at each sample is calculated for current, denoised antenna and filter output by considering a window of 40 samples	38
Figure 30: Peak values of the denoised antenna and filter output are compared with signals themselves to find the regions of peak and then signals to noise ratio is determined for the two signals based on these regions of the peak (PD) and noise (no PD).....	39
Figure 31: All the variables calculated within the program for each level of applied impulse voltage are written along with headers to an excel spreadsheet named and located by the user..	39
Figure 32: Picture of experimental setup used for PD test without grounded steel plate	40
Figure 33: Top view of Experimental setup showing connections made using grounded steel plate using antenna.....	41

I. INTRODUCTION

A partial discharge (PD) occurs within the insulation material when a high voltage stresses it, initiating ionization within imperfections/voids of the insulation because of the lower dielectric strength of the void compared to insulation material. When the voltage across the insulation approaches its peak value, these discharges partially bridge the gap between imperfection and the ground and attenuate quickly due to its high frequency [1].

When PD continues to cause ionization within the imperfection/void, it causes local heating and carbonization. If the same insulation, under the voltage stress, is continued to be used, the progressive carbonization/ tracking will ultimately lead to complete breakdown of insulation when an arc completely bridges the gap between conductor and ground [1].

With the rapidly increasing use of PWM inverter-fed machines, detecting PD events at an early stage has become very important for industries in order to avoid downtime caused due to insulation failure [3-5]. Hence, PD detection is seen as a preventive measure to check the health of insulation before installation or to predict the remaining life of insulation after a certain period of use [2].

The PD signals have a high-frequency bandwidth ranging from a few to hundreds of MHz. In the presence of high-frequency noise, it becomes difficult to get a clean PD detection. High-frequency noise, if present, also makes it challenging to define thresholds for the PD levels, hence making PD detection scheme ineffective to detect smaller PD events [6].

In this work, we concentrated on PD detection in stator insulation of medium voltage AC machines. A reliable detection method which utilizes two independent detection schemes is presented.

II. BACKGROUND

2.1 Partial Discharge

Partial Discharge (PD) is an electric discharge that partially bridges the insulation gap between phase to phase or phase to ground. The imperfections/voids present within the insulation have lower dielectric strength as compared to that of insulation material. When a high voltage appears across an insulation, the insulation material bears the electric stress due to its high breakdown strength, but the void undergoes local breakdown with a transient gaseous ionization as the electric stress exceeds the critical value, resulting in PD. The discharges occur in form of small arcs, which deteriorate the insulation and may eventually lead to its complete breakdown.

When initiated, PD gives rise to high frequency transient current pulses, which persist for short duration ranging from few nanoseconds to a microsecond. These discharges appear near the peak of the applied voltage, then disappear and reappear repeatedly after voltage goes through zero crossing.

The PD sites may be located anywhere between the copper conductor and insulation wall, or internal to the insulation itself, between the outer insulation wall and ground, or along the surface of the insulation. These sites may be a result of many factors such as machine design process, manufacturing methods, insulation material, operating conditions or maintenance practices. The form of PD depends on many features of the discharge site within insulation, such as size and shape of cavity, gas, and pressure within the void, nature of surface etc. PD activity is observed in many forms such as electrical pulses, radio frequency (RF) emissions, acoustic pulses, or light/glow. These features of PD have been used in past to measure and detect them within stator winding or other electric machines [12].

The magnitude of PD corresponds to the extent of damage caused by the insulation and,

hence, proves to be an important factor to predict the health of the insulation under test. This has led to the invention of various PD detection and measurement schemes during the last century.

Some of the PD detection techniques developed in the past used the integral of PD currents, measured in pico-coulombs (pC) to measure PD signal magnitude by using analog oscilloscope [6], by calculating the charge transferred [9] or by implementing a factory measurement system using a shielded room [10]. However, through recent advancements in PD testing measures, along with better digital signal processing technologies, PD can now be measured at the terminals in millivolts (mV) instead of pC, which presented calibration problems earlier [11].

Many detection schemes have been proposed in the past, such as detection of PD using a coupling capacitor between a high voltage source and a machine under test [6-8], detection based on the broadband impedance of the motor (from 10 kHz up to 9.5 MHz) [7], and hi-pass filtering [8] (frequency not mentioned). The physical attributes of discharge such as electromagnetic radiation sensed using an RF antenna [14-15], acoustic noise, and visible and UV light emissions, have also been used to sense discharges within the test insulation in many PD sensing techniques [6,12]. Ultra wide band (UWB) detection, using the wavelet transform, has also become popular in recent years to extract PD signals from the terminal voltage of IGBT driven motors [16].

As depicted in figure 1, measuring the terminal voltage during discharges and extracting information about the PD level using a filter [16] is highly dependent on the internal impedances of the high voltage source (impulse generator), the connections, and the distributed inductances and capacitances of motor under test as seen from the point of measurement [7].

On the other hand, radiation due to PD measured by an antenna is unaffected by these impedances as it measures not the terminal voltage but electromagnetic radiation from actual discharge currents taking place inside the insulation.

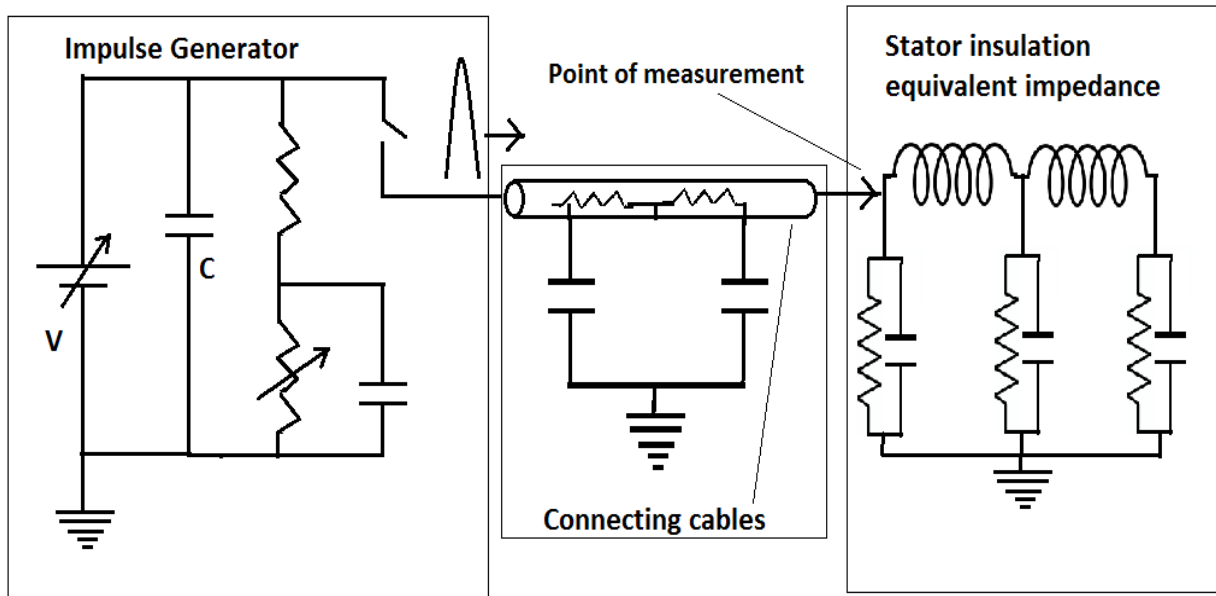


Figure 1: Impedance diagram of PD test setups, which use voltage measurements techniques

It is hard to rely entirely on results from a PD detection method based on just one PD sensor/detector to make a confident decision on the presence of PD [13]. Even if there is no PD, some noise in the output signal may exceed the threshold reference set for low-level PDs. Moreover, in such a case, one cannot be sure whether the detector is malfunctioning or produces faulty results.

PD detection techniques already published [17-19] have provided ample evidence to support the idea that an antenna can be used efficiently to recognize PD events by denoising the signals using the wavelet transform. Some of these techniques used artificial defect models as laboratory setups by carrying out feature extraction of PD (applicable to GIS and transformer insulation) through kernel principal component analysis (KPCA) [17], or by deploying four different types of antennas to sense PD events [18]. Some researchers also presented methods which used artificial defect models like point-plane arrangements to produce PD signals and then denoised them using undecimated wavelet transform (UWT) through data mining procedures [20] or through probabilistic principal component analysis (PPCA)[22].

In order to enhance the reliability in the decision-making process for PD detection, a new PD detection technique is presented, with two independent schemes simultaneously detecting PD events. A filter (PD separator) is used as one independent scheme to detect PD at the terminal of a motor, which works simultaneously with another independent detection scheme in which an antenna provides no contact detection of PD events by sensing the electromagnetic radiation caused by discharge currents. Some grounding arrangements were devised to minimize the system and background noise during the test, enabling the antenna to measure PD by sensing the electromagnetic radiation caused by discharge currents without any interference.

The objective of this work was to develop an accurate and repeatable standard technique to test actual medium voltage stators for any presence of PD when tested by applied high voltage impulses. It is demonstrated that the developed method provides high confidence to declare if a stator under test is affected by the presence of PD or healthy to use for a normal operation.

2.2 Wavelet Transform

In the process to detect the presence of PD, the wavelet transform was preferred over other signal processing techniques to denoise both filter and antenna signals because localization of PD in the time domain was necessary due to the non-stationary nature of PD. Since a wavelet transform can provide time and location representation of the signal simultaneously, it suited well to PD extraction requirements.

Another reason to choose the wavelet transform is that the frequency at which partial discharges occur is not fixed and can be anywhere from kHz to hundreds of MHz. Hence, a robust signal-processing tool, which can identify these events by not limiting the bandwidth of detection, is required.

The wavelet transform is performed on a time-domain signal by decomposing it using a series of cascaded filter banks. In other words, the signal gets split with the help of translated and dilated wavelets.

A wavelet represents a wave-like oscillation with an amplitude that begins at zero, increases up to a maximum value, with oscillations, and decreases back to zero. It is a normalized function with zero average value [22]. The family of wavelet used for this work to extract PD is the Daubechies family. A typical representation of wavelet and scaling functions of Daubechies 14 and Daubechies 4 are as shown in figure 2. It is these properties of being irregular in shape and compactly supported that make wavelets an ideal tool for analyzing signals of a non-stationary nature.

Unlike the Fourier transform, which uses sinusoids, that carry infinite energy spread across time as basis function, the wavelet transform uses unique basis functions with finite energy concentrated around a point in the time scale.

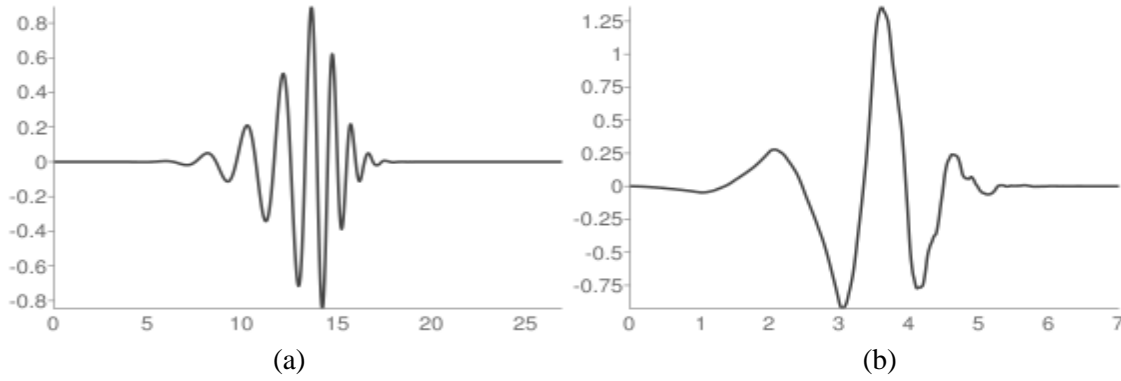


Figure 2: Wavelet function for Daubechies 14(db14) (a) and Daubechies 4(db4) (b)

Mathematically, the wavelet transform is defined by the equation [20]:

$$\Psi(s, \tau) = \int_{-\infty}^{\infty} f(t)\psi^*(s, \tau)dt$$

where s is the scale and τ is the translation and

$$\psi(s, \tau) = \frac{1}{\sqrt{s}} \frac{(t - \tau)}{s}$$

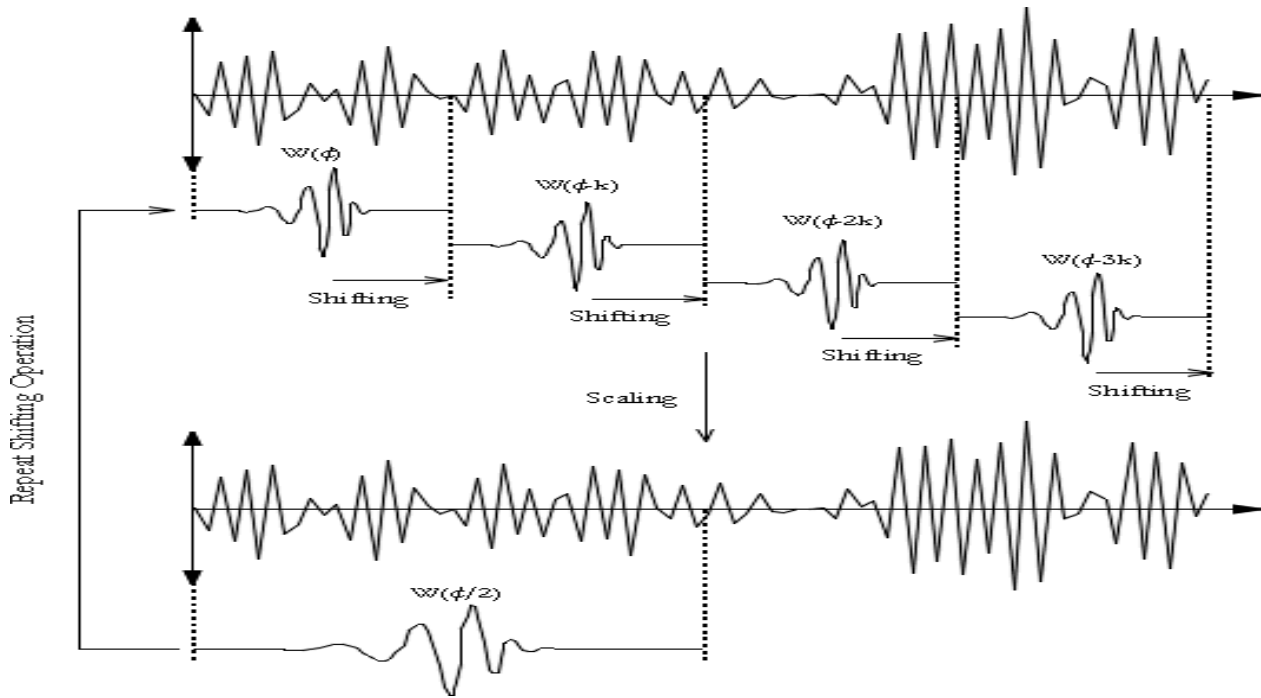


Figure 3: Scaling and shifting process during decomposition of signal using UWT (credits: <http://www.wavelet.org/tutorial/wbasic.htm>)

In the process of wavelet transformation, coefficients are calculated which represent the correlation between the wavelet and local sections of the signal by applying translations (shifting) and dilations (scaling) to the wavelet as shown in figure 3.

The scaling or dilation process can be expressed as a tree of low and high pass filter banks as shown in figure 4. The low pass filters, $G_1(z)$ output the approximation coefficients ($A_1, A_2 \dots A_L$) and high pass filters, $G_0(z)$ output detail coefficients ($D_1, D_2 \dots D_L$), respectively.

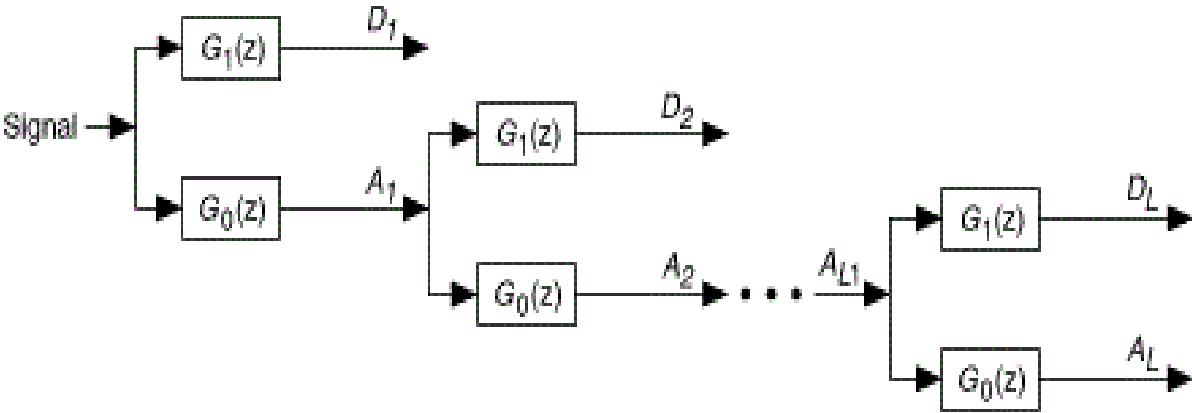


Figure 4: Scaling/dilation process for UWT, explained by filter bank algorithm (credits: http://zone.ni.com/reference/en-XX/help/371419D-01/lvasptconcepts/wa_dwt/)

Unlike other variants of wavelet transforms, the Undecimated Wavelet Transform (UWT) displays translation invariance, or a shift invariant property, which provides time localization of PD, assisting the feature extraction process. Technically, UWT has detail and approximation coefficients of the same length at every decomposition level as downsampling is not involved at all. Hence, the higher the decomposition level, the lower is the resolution of UWT due to dilation at each step.

The UWT process can be applied in reverse to reconstruct the signals from the UWT

coefficients ($D_1, D_2 \dots D_L$) as shown in figure 5. This process inverse UWT gives the required denoised waveform after the rejection of undesired levels (scales) from the decompositions shown in figure 5.

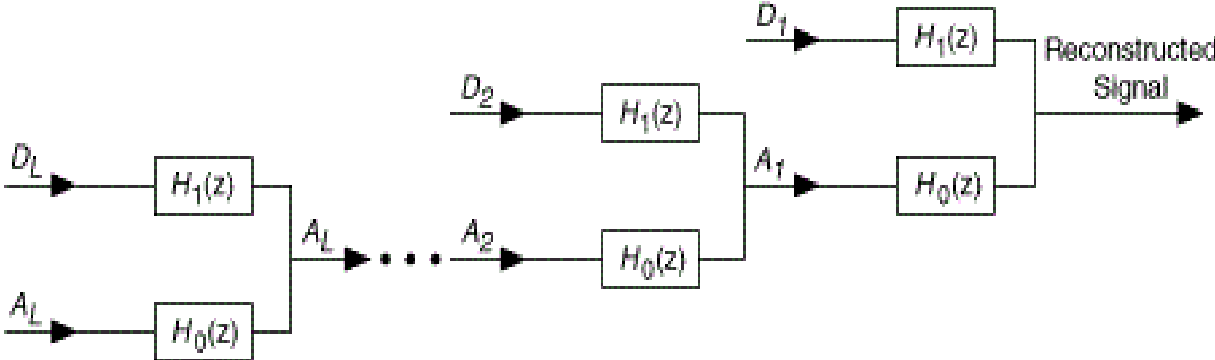


Figure 5: Signal Reconstruction using inverse- UWT, explained by filter bank algorithm (credits: http://zone.ni.com/reference/en-XX/help/371419D-01/lvasptconcepts/wa_dwt/)

The process of denoising using a UWT is explained in the following steps:

1. The signal to be denoised is first decomposed into L levels by first selecting a particular wavelet and then by performing the dilation and shifting process as shown in figure 3
2. Amongst the wavelet coefficients obtained, coefficients related to noise and signal details are identified and separated
3. The coefficients showing good signal strength are reconstructed using inverse-UWT process, whereas coefficients representing noise are excluded from reconstruction.

Hence, the denoised signal after UWT and inverse UWT transform will be free from noisy components observed during the decomposition process.

2.3 Linear Discriminant Analysis

The Linear Discriminant Analysis (LDA) [23] is a machine learning and pattern recognition tool, which takes the data to be classified as input and categorizes it based on a linear combination of its features. This technique can be used for the dimension reduction and classification of any linearly separable data. It helps to categorize points lying in a multidimensional space into separate disjoint regions with the help of calculated weighting coefficients for each region.

If data with two features is to be categorized into two classes. They can be plotted as shown in figure 6, with each axes representing one feature. In order to ensure maximum separation between data for class1 (red) and class2 (green), a separate axis y is chosen such that separation between the mean of two classes is maximum, whereas variance within the classes is minimum.

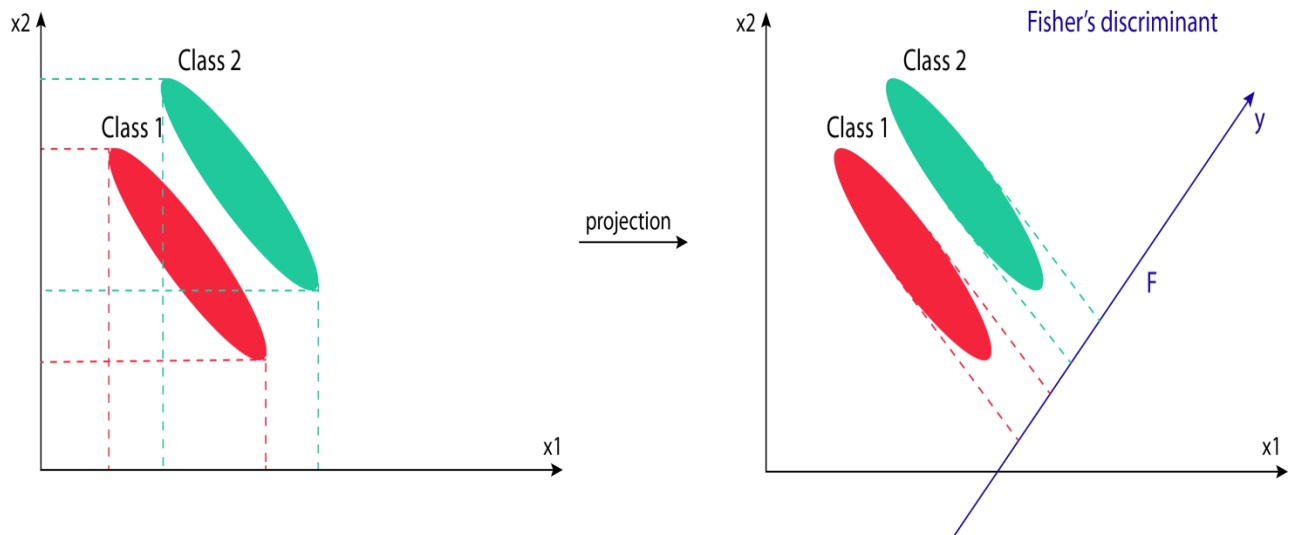


Figure 6: Linear Discriminant Analysis to maximize separability between two classes (credits:<http://www.coxdocs.org/doku.php?id=perseus:user:activities:matrixprocessing:learning:classificationfeatureselection>)

Let us consider a general case where we want to categorize a d -dimensional dataset into

two classes by projecting it onto a k-dimensional subspace (where $k < d$). First, the within-class scatter S_W and between class S_B scatter are calculated as follows:

$$S_W = \sum_{i=1}^c \sum_{x_k \in X_i} (x_k - \mu_i)(x_k - \mu_i)^t$$

$$S_B = \sum_{i=1}^c N_i(\mu_i - \mu)(\mu_i - \mu)^t$$

Where C is the number of classes, X_i is the set of all points that fall into class i , μ_i is the mean of class i , x_k is the k th point of X_i , N_i is the mean of class i , μ_i is the mean of class i and μ is the overall mean

LDA maximizes the ratio of between-class variance to the within-class variance of the considered dataset thereby allowing maximum separability among classes. One way to do this is to find the eigenvectors of $S_W^{-1}S_B$ and select C eigenvectors corresponding to C highest eigenvalues. These C eigenvalues form a transformational matrix W such that:

$$Y = W^t X + W_0$$

The Y matrix is the new K -dimensional dataset, obtained by using the original dataset as the matrix X and the matrix W calculated in last step and W_0 is a bias constant. The plot for matrix Y will represent the dataset with maximum separability in the reduced dimensions.

The classification of data based on their features is possible through linear discriminant functions. An N -dimensional sample space is categorized into K classes, based on weighting coefficients of discriminant functions for all classes as follows:

$$D_k(x) = x_1 a_{1k} + x_2 a_{2k} + \dots + x_N a_{Nk} + a_{N+1}, k = 1, 2, \dots, K,$$

where a_{ik} represents the normalized i -th weighting coefficient for k -th class and x is the N -dimensional

vector to be classified. To determine whether a particular sample vector x_i belongs to the j -th class, we check if its discriminant function is greater than for any other classes:

$$\mathbf{a}_j^T \mathbf{x}_i > \mathbf{a}_l^T \mathbf{x}_i \dots \text{for every } i \neq l$$

where \mathbf{a}_j^T and \mathbf{a}_l^T are the transformed coefficient vectors for class j and l , respectively.

To find the weighting coefficients, which form the discriminant function for all classes, a training procedure was followed which adjusts these coefficients (pre-assumed) to end up with the required classification of data samples. The training algorithm should converge for a linearly separable dataset, over a finite number of steps. If the discriminant functions classify the sample vector correctly, no adjustment is made to the weighing coefficients. In the case of incorrect classification, the weights of the discriminant functions are adjusted according to following rule:

$$\text{If } \mathbf{a}_j^T \mathbf{x}_i \leq \mathbf{a}_l^T \mathbf{x}_i \dots \text{for every } i \neq l$$

$$\text{where } \mathbf{a}_l^T \mathbf{x}_i = \max_{l \neq j} [\mathbf{a}_1^T \mathbf{x}_i, \dots, \mathbf{a}_k^T \mathbf{x}_i],$$

weighing coefficients for vectors \mathbf{a}_j and \mathbf{a}_l are calculated for the next step as:

$$\mathbf{a}_j(i+1) = \mathbf{a}_j(i) + \mathbf{x}_i$$

$$\text{and } \mathbf{a}_l(i+1) = \mathbf{a}_l(i) + \mathbf{x}_i$$

Whereas, other coefficients are kept the same.

2.4 Hilbert Transform and Envelope Detection

In some cases, it becomes necessary to find the envelopes of two signals before correlating them. In order to extract the envelope using analytic signal, the Hilbert transform is applied to the signal. Hilbert transform of a function $x(t)$ is mathematically represented as follows:

$$h(t) = H\{x(t)\} = \frac{1}{\pi} \int_{-\infty}^{\infty} \frac{x(\tau)}{t - \tau} d\tau$$

Fourier transform of the Hilbert transform of $x(t)$ is given by:

$$H(f) = -j * \text{sgn}(f) * X(f)$$

where, $H(f)$ and $X(f)$ are Fourier transforms of $h(t)$ and $x(t)$ respectively

To perform discrete implementation of Hilbert transform on the given signal, FFT routines are followed to perform the Hilbert transform in following steps:

1. The Fourier transform (Y) is calculated for the given signal (X)
2. The DC component (Y_0) is set to zero
3. The Nyquist components are set to zero if Y is even in size
4. The positive harmonic components are multiplied by $-j$
5. The negative harmonic components are multiplied by j and the output is labeled as H , which is nothing but $H_m = -j * \text{sgn}(m) * Y_m$
6. Inverse Fourier Transform is applied to H to get Hilbert transform of X

Once we have the Hilbert transform $h(t)$ for real data signal $x(t)$, we calculate analytic signal as follows:

$$a(t) = x(t) + i * h(t)$$

The magnitude of this complex function $a(t)$, provides an instantaneous magnitude of the analytic signal and can be expressed as:

$$A(t) = \sqrt{x(t)^2 + h(t)^2}$$

Here $A(t)$ represents extracted envelope of real data signal $x(t)$ using analytic signal $a(t)$

III. WORK PERFORMED

The details of the PD detection technique developed are discussed in this section. An attempt was made to standardize PD testing for medium voltage stators. This class of stators is exposed to 60 Hz high voltage produced by Pulse Width Modulated (PWM) drives, required for variable speed-torque operation. But along with the 60 Hz operating voltage, high voltage peaks with very short rise time (impulse voltages) are also produced. These impulse voltages appear at the input of stator due to switching operations within PWM drives and are sufficient to produce high voltage stress, which initiates PD within the insulation.

At present, attention is given towards PD testing technique using impulse voltages. An attempt is made to develop a standard technique using impulse high voltage, to examine the health of a medium voltage stator by accurately checking for the presence of PD.

The test setup first used in the laboratory is discussed in detail. Later, some modifications were made which help reduce background noise. Considering that the automation of the test procedure was necessary for its standardization, an algorithm was developed in the LabVIEW environment which may be implemented for every test for PD for any stator.

Results are discussed and comparisons are made at the end of the thesis to show improvements achieved at each step. The results from the developed PD technique shows the high repeatability and accuracy required of a standard test procedure.

3.1 Experimental Setup

During the developing stages of the PD detection technique for medium voltage stator insulation, an IRIS Power PDA-IV instrument was used as a filter to extract high-frequency partial discharges from the high voltage present at the terminals of the stator windings as shown in figure 7. A Baker (DTO5-3) instrument was used as an impulse generator, producing high voltage impulses with a very short rise time of 2 μ s. These high voltage impulses applied to the stator represent the high voltage peaks with short rise time which are produced by a PWM drive controlling a variable speed/torque motor.

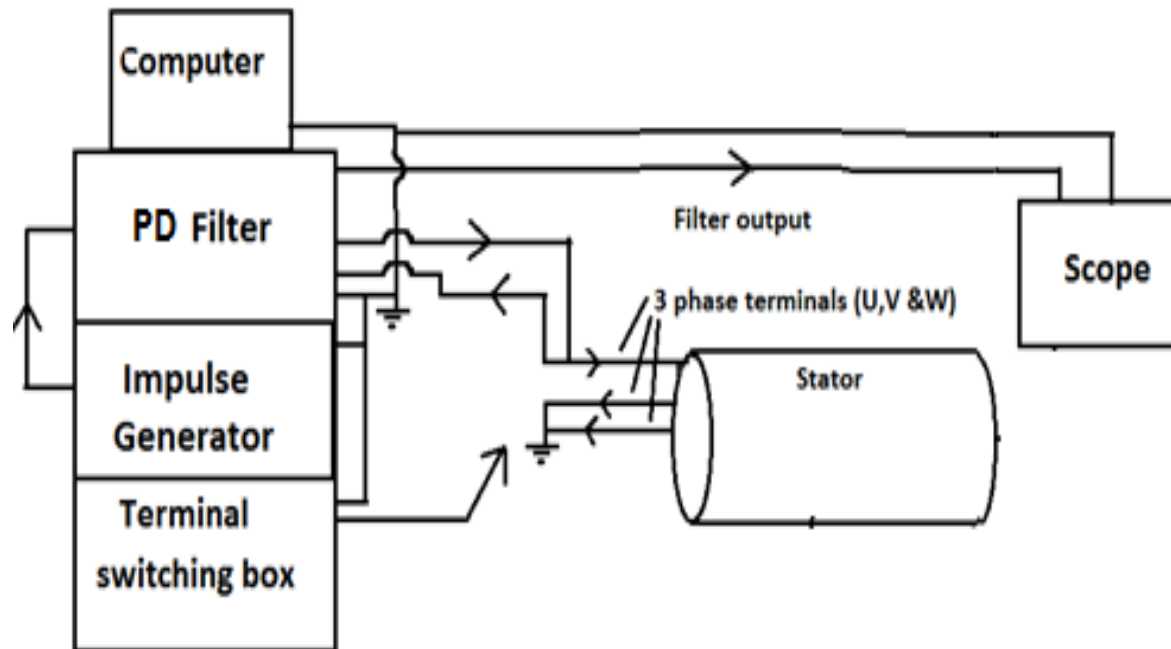


Figure 7: Laboratory setup for PD detection using filter at stator ends

To provide an alternative and to make the combined detection of PD caused by an impulse voltage more accurate and reliable, an antenna was positioned on the axis of the stator to record PD

events along with the filter, which served as second independent tool for detection as seen in figure

8

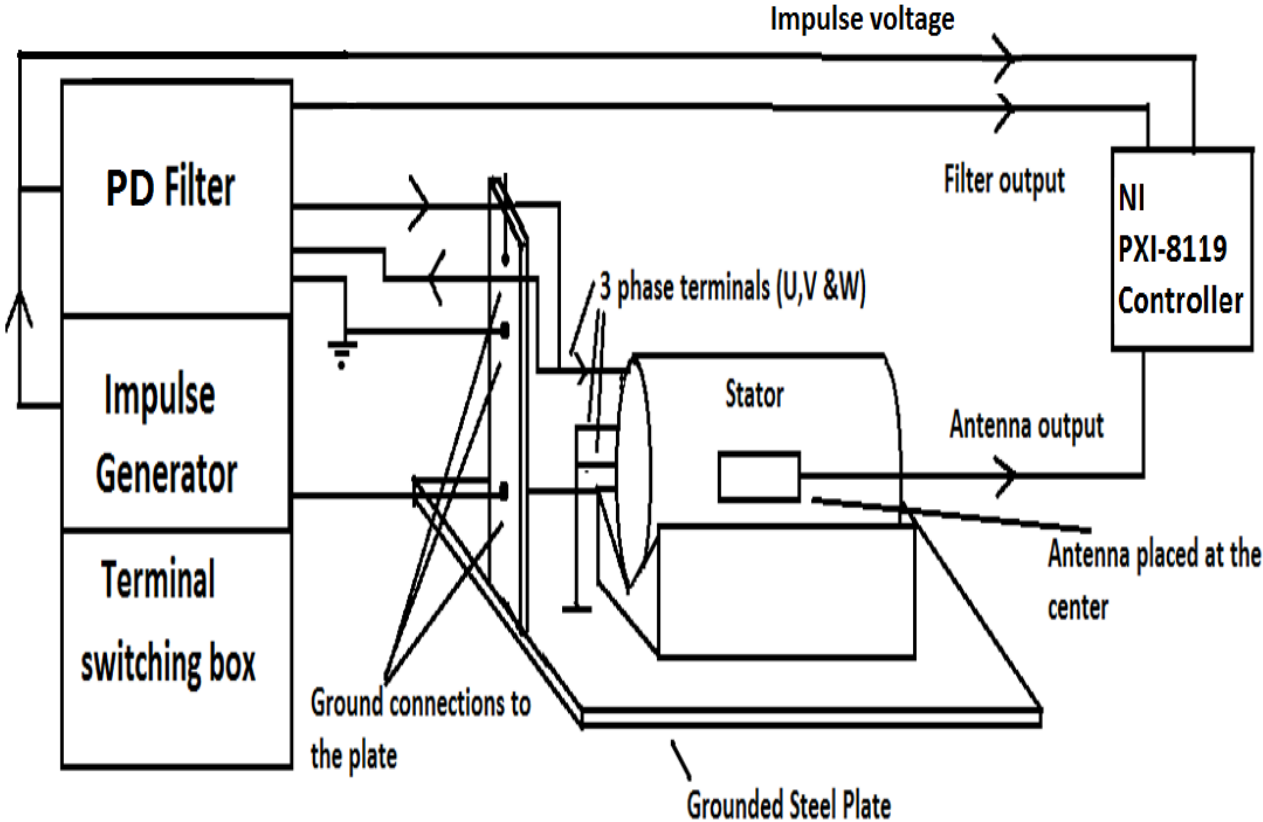


Figure 8: Grounded steel plate setup block diagram for reliable PD detection using filter and an antenna simultaneously

To minimize the system noise and interference, a common grounding steel plate was placed as shown in figure 8 and 9. The plate served the purpose of common grounding node for all the equipment used for PD detection. The connecting leads were kept short in length and were laid parallel to the common grounding plate to minimize the interference due to the inductive effect (figure 9).

To collect a large amount of test data and analyze them quickly and effectively, a data acquisition system was set up using an NI PXI 8119 controller to acquire the desired signals, namely the applied impulse voltage (L-G), ground current, raw filter output and raw antenna output.

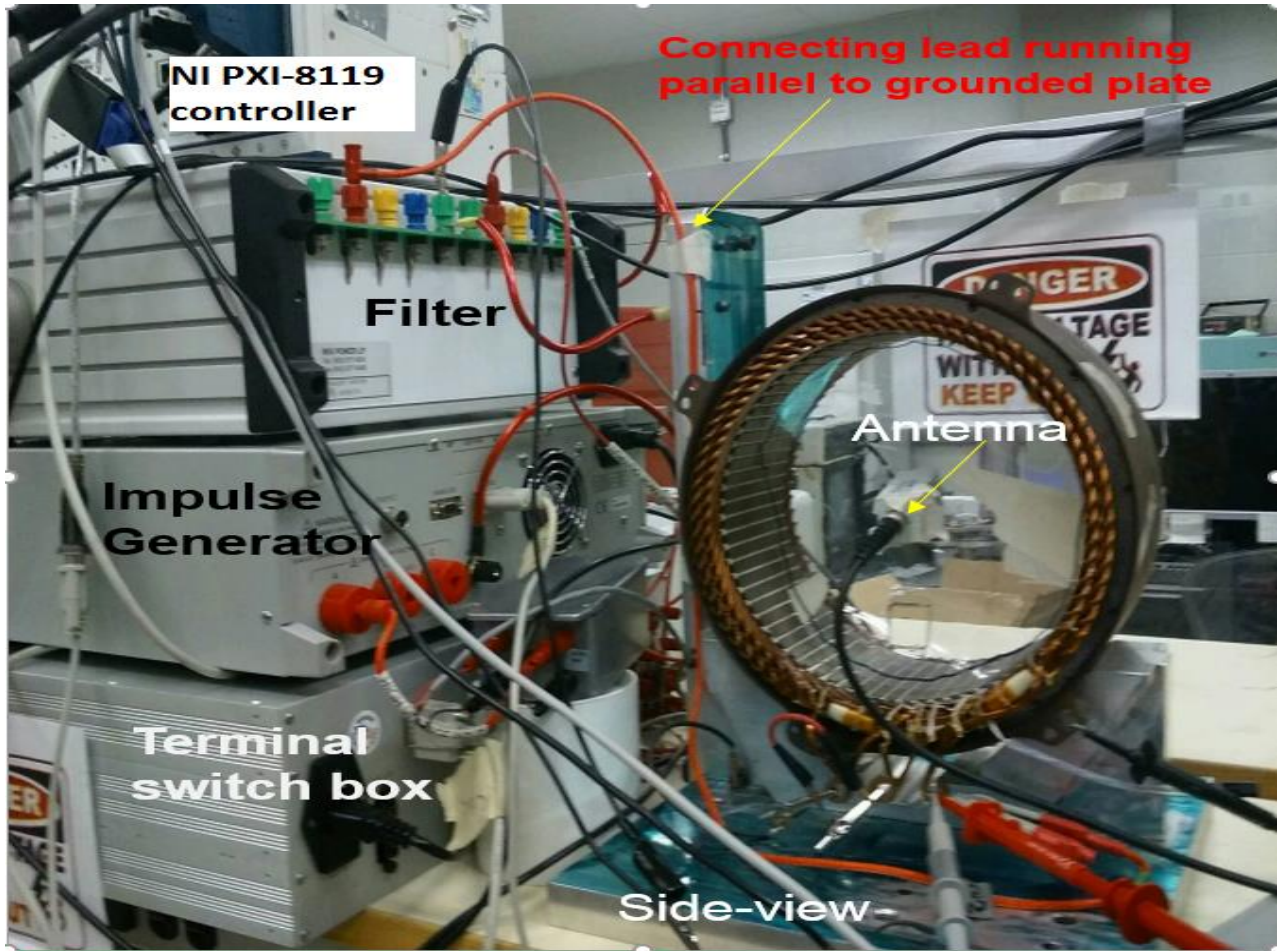


Figure 9: Grounded steel plate actual setup for reliable PD detection using filter and an antenna simultaneously

To capture every detail of the signal provided by the antenna, it was decided to examine the raw signal first, by not tuning it to any particular frequency band. Hence, the signal from the antenna, placed as shown in figure 9, was sampled directly without applying any signal processing technique. The antenna was positioned approximately at the mid-length of the stator (axis midpoint), and at a variety of positions between the axis and circumference of the stator.

3.2 Signal Conditioning in LabVIEW

3.2.1 Extraction of Partial Discharge signal

A high voltage impulse between 500V and 3 kV (0.5 MHz), shown in figure 10C, was applied to the stator. The voltage output of the filter (figure 10A) shows the extracted PD events from the terminal voltage of the stator. The antenna sensed the discharges at the same time by capturing the electromagnetic radiation due to the discharge current (figure 10B). The output signals from impulse generator, filter and antenna were digitized (0.5 G-samples/s) using NI PXI 5152 cards on a PXI 8119 controller and later analyzed together using LabVIEW, as shown in figure 9.

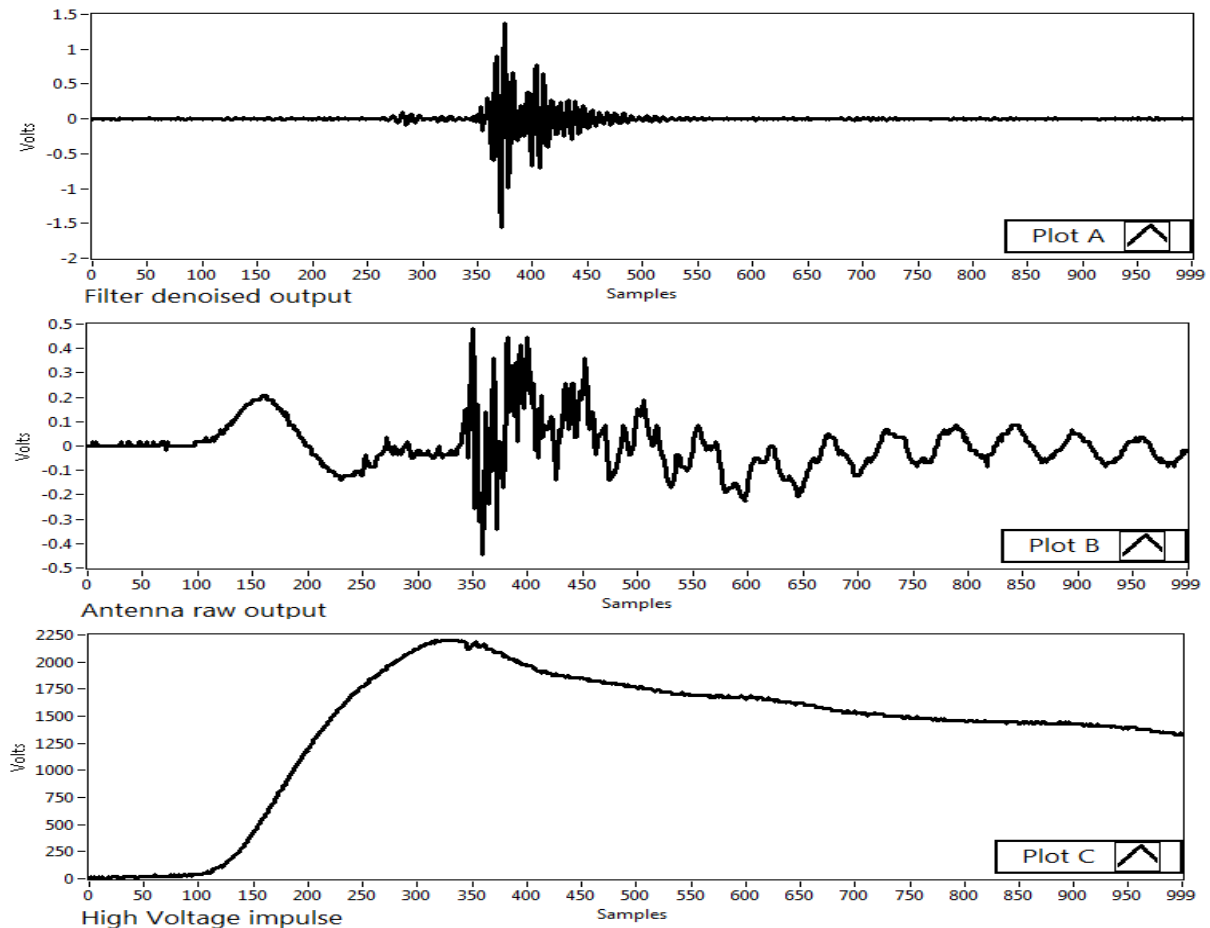


Figure 10: PD test response from filter (A), antenna (B) for applied impulse of 2.25KV (C) from test setup shown in figure 2 and 3

As seen in figure 10, the filter produces an output detected as PD around the 350th sample. This instance corresponds to the peak of the applied HV impulse (plot C), whereas the antenna raw output (plot B) appears too noisy, making it difficult to spot the PD event, which roughly starts around 350th sample. Therefore, the raw signals from antenna were de-noised using discrete wavelets transform (DWT) to extract cleaner PD signals, as shown in figure 9.

By applying a multilevel undecimated wavelet transform (Daubechies 4) to the raw antenna output (figure 11A), the antenna signal was decomposed into six levels. The selected level 4 was adequate to extract the PD component from the raw antenna signal (figure 11B).

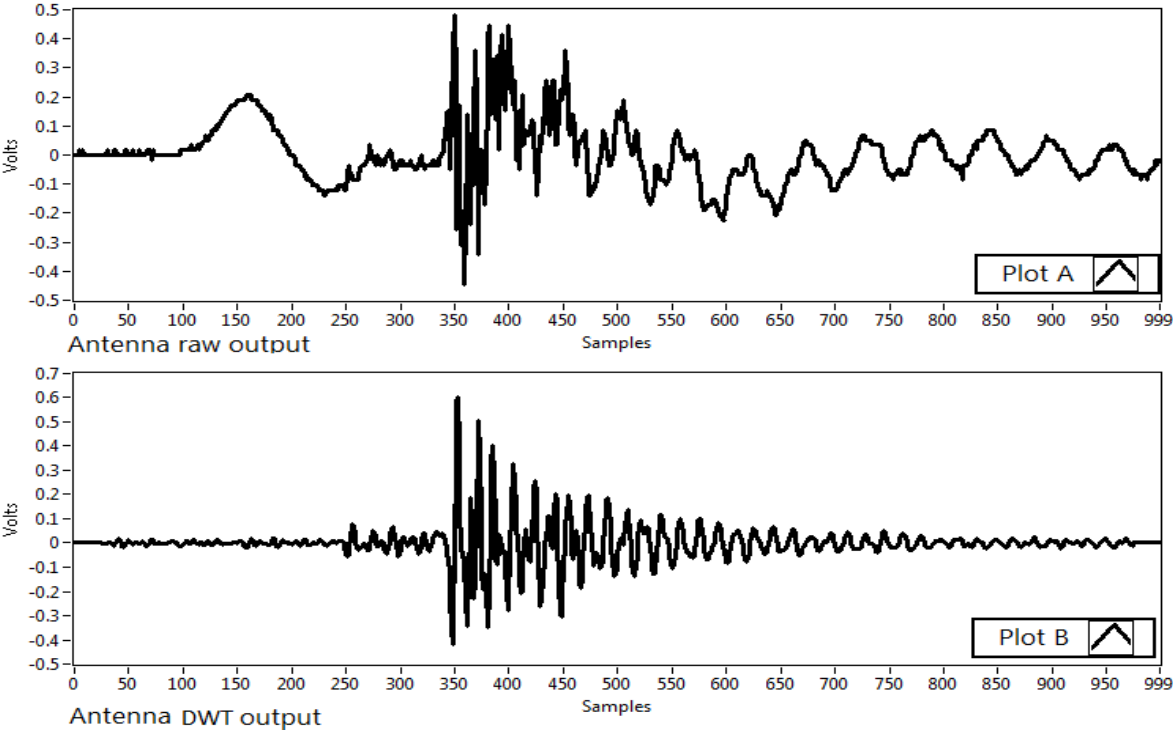


Figure 11: Raw PD response on antenna (A) and extracted PD signal from antenna (B)

As seen from above, the output of the filter (figure 10A) and the antenna output signal after UDWT operation (figure 11B) could be used simultaneously to confirm the presence of PD for the applied impulse voltage around the 350th sample, and hence presents a reliable way to sense PD activity inside a stator under test.

3.2.2 Second Level Denoising process

While testing some stators for PD, some cases were observed, shown in figure 12, where the raw output of the filter was influenced by noise with different characteristics when compared to PD. The presence of noise between the 50th to 250th samples in the filter output affected the ability to set accurately a threshold for the PD detection.

To denoise the raw filter output (figure 12A), it was decomposed into 10 levels using Daubechies 14 wavelet. Subsequently levels 8 and 9 were used to reconstruct the signal using the inverse undecimated wavelet transform, which provided the desired cleaner PD detection as shown in figure 12B.

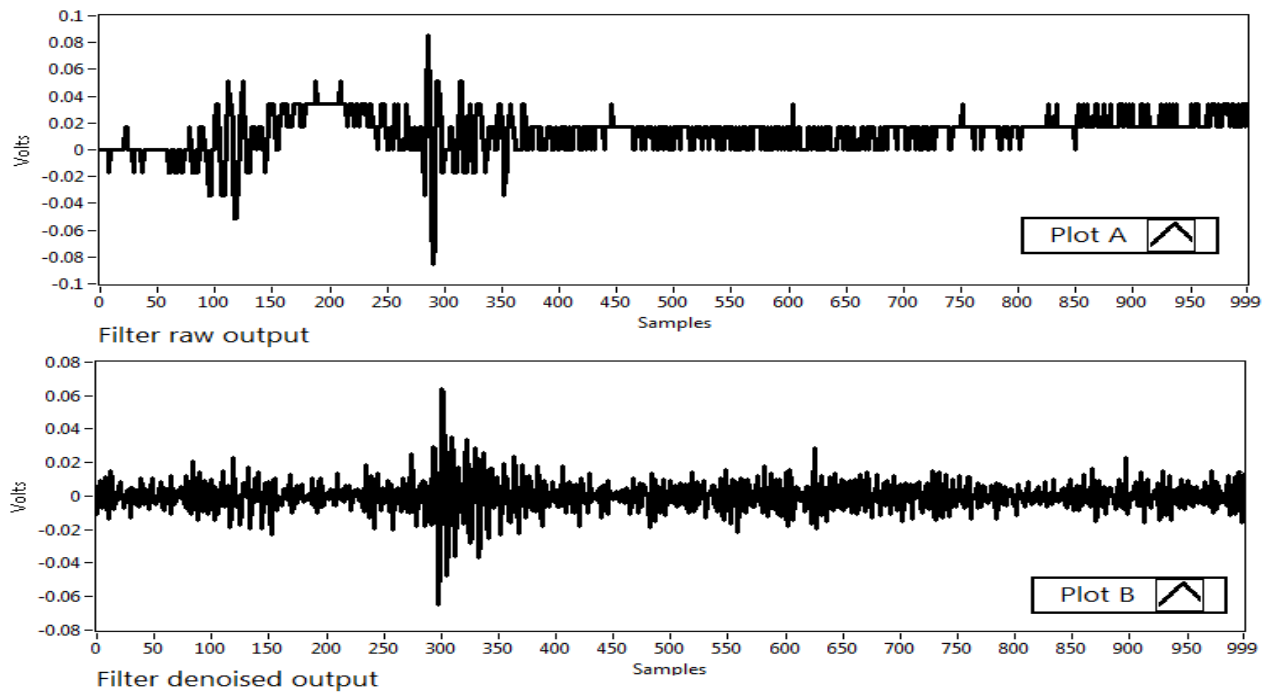


Figure 12: Comparison between PD response of filter before denoising (A) and after denoising (B)

On some occasions, the antenna output, even after UDWT processing had some spurious random peaks such as the one shown in figure 13. As these noisy peaks exceeded in some cases the threshold reference set for antenna and signaled false PD, it became necessary to eliminate them. On

observing that such noise lasted for at most 80 ns, which was much shorter than that of the actual PD, such cases were separated based on the duration of the peaks in the antenna output.

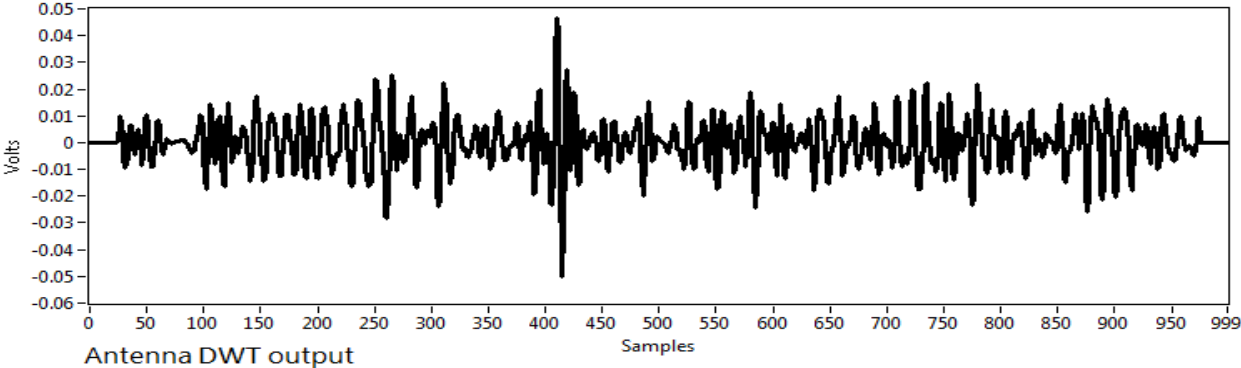


Figure 13: Noisy peak in DWT treated antenna output

IV. EXPERIMENTAL PROCEDURE

As the PD tests were to be carried out more than once for each of the different kinds of stators, it was not feasible to initially conduct the analysis manually inspecting the waveforms after each test. In order to automate the PD detection process, an algorithm was programmed in LabVIEW. Its flowchart is shown in figure 14, which can process a large amount of test data and perform the PD detection process efficiently.

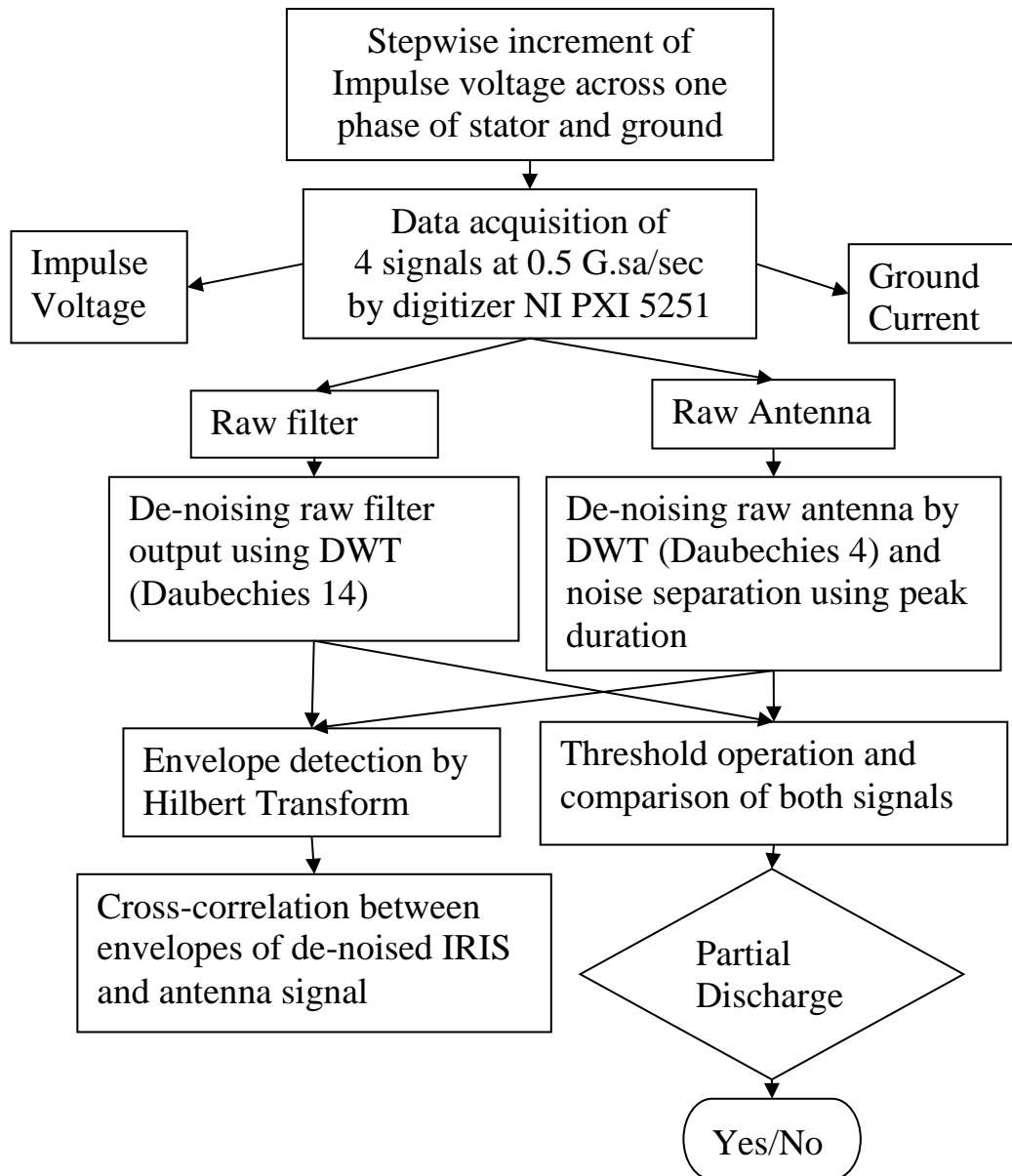


Figure 14: Flow Chart showing Signal Reconditioning process in LabVIEW.

The stator was tested for PD by applying a train of impulses starting from a few hundred volts up to 3.0 to 3.5 KV with a frequency of 0.5 MHz. The waveforms to be analyzed, the applied impulse voltage, ground current, raw antenna output and raw filter output, were sampled as 0.5 Gsa /second. The high sampling rate was required to capture the high-frequency PD activities of interest and to avoid loss of any information.

After sampling both signals, the waveforms of each, the filter and antenna were denoised using wavelets and the wavelet processed antenna output was treated further to remove spurious noise peaks by applying the peak duration algorithm.

The de-noised waveforms of the filter and antenna were then compared to predetermined thresholds, which were used to detect the presence of PD. To decide on threshold reference levels for the filtered outputs of the antenna and the IRIS filter, the maximum peak value of noise

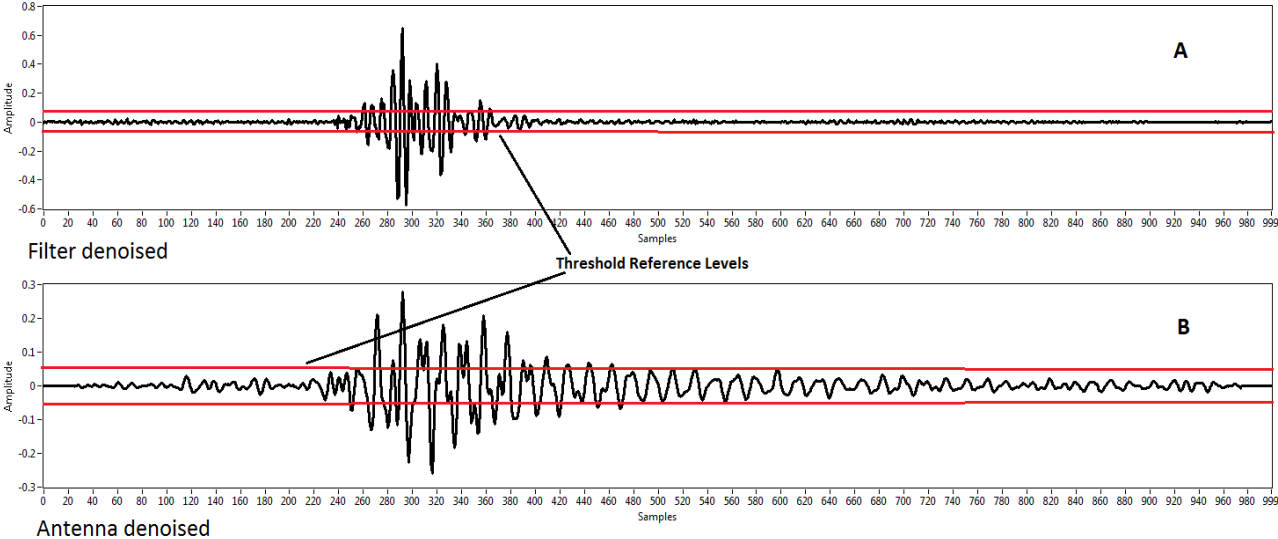


Figure 15: Threshold reference levels for filter (A) and antenna (B) outputs

was calculated for the data from five different stators below the PD inception voltages for both filter and antenna. After considering a safety margin of 40 mV, the threshold reference levels for the filter and antenna were set at 170 mV and 100 mV respectively (figure 15).

The decision on the presence of PD was based on denoised signals from both the filter and antenna. If both agreed on the presence or absence of PD for any applied impulse, that was considered as a reliable determination of PD.

Along with the threshold process, a cross-correlation of de-noised IRIS signal with that of the de-noised antenna was performed. Prior to this correlation, Hilbert transform was applied to both waveforms to extract their envelopes. An example of the correlation process is shown in figure 16.

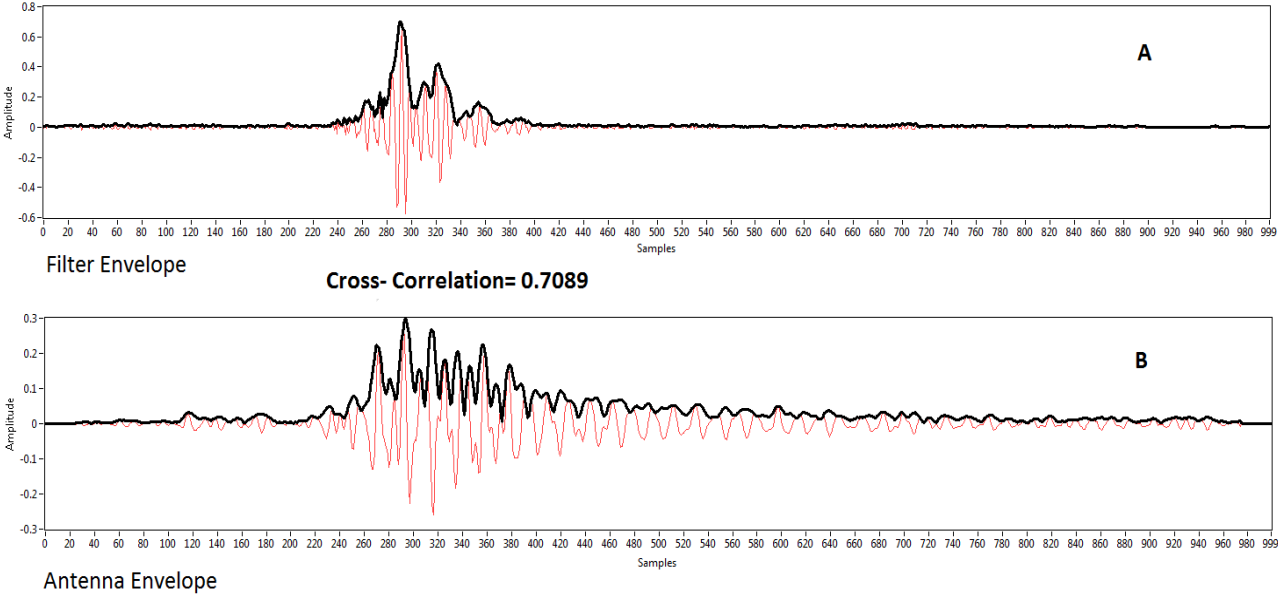
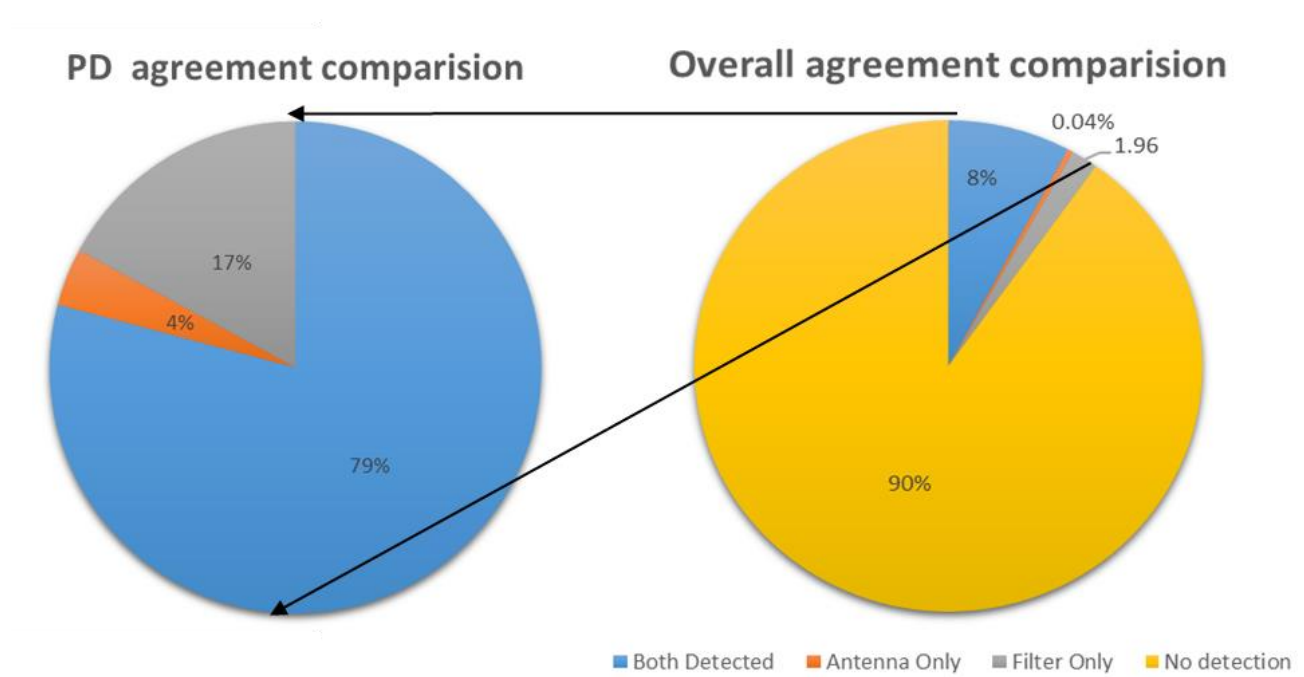


Figure 16: Envelope extraction of filter (A) and antenna (B) outputs

Hence, the similarity between the filter and antenna signals (figure 15) resulted in a cross-correlation factor of 0.7089 (figure 16). By correlating the envelopes, the shape of the two signals was compared without being affected by arbitrary noise levels, making the calculation effective. Therefore, correlation calculation serves as a second tool after the threshold process has been applied, to determine the similarity between the denoised outputs of the antenna and the filter.

V. EXPERIMENTAL RESULTS

The simplest way to evaluate the accuracy of the proposed technique was to calculate the agreement percentage based on decisions made by the filter and antenna outputs, for each applied impulse voltage. A low percentage of disagreements was expected between the two PD indicators, in order to confirm the reliability of the combined detection scheme.



Before correction			After correction		
Voltage level	Filter	Antenna	Voltage level	Filter	Antenna
V-dv	PD	PD	V-dv	PD	PD
V	PD	Noise	V	PD	PD
V+dv	PD	PD	V+dv	PD	PD

Figure 17: Overall agreement comparison and PD agreement comparison and correction logic

When using the output of the filter and of the antenna for a specific impulse level leads to divergent decisions, as in Fig 17, the results are re-evaluated. The decision is then based on the outputs of the antenna and the filter at voltage levels differing by one voltage step, i.e. for voltage level V for one and $V \pm dv$ for the other. This is to decrease the effect of low noise and slight differences in the thresholds used for the two decision systems. This technique improved the agreement between the decisions using the two outputs from 68.5 % to 79 % in a typical case.

The algorithm developed in LabVIEW as shown in the flowchart (figure 14), along with the above correction, was applied to the test data from 13 different stators tested between 05/25/2016 and 09/02/2016 at General Motors facility, with variation in phase under test, axial antenna position and the inner diameter of the stator. The stators were selected from the trial production line with externally introduced defects to create PD.

It can be seen from the overall agreement comparison shown in figure 17 that, the cases with no PD detection on both antenna and filter cover most of the area (90%) in the pie-chart. This is obvious as there will be no disagreements between them as long as there is no PD initiated while testing with low voltages. Therefore, in order to make the comparison more relevant and realistic, these cases of no PD detections were left out and remaining cases were studied in the form of PD agreement comparison. This way, it becomes clear that both filter and antenna detected PD on 79 % of the cases. Whereas, 21 % of the cases showed disagreement on the presence of PD.

To see how the introduction of the grounded metal plate improved PD detection, the outputs of filter and antenna were compared for both cases as shown in figure 20. The PD detections, with the grounded steel plate in place, were found to be much cleaner on antenna and filter. The level of noise in the antenna output for the test setup with no steel plate (right side) was found to be higher than the noise levels with the grounded steel plate (left side). Hence, the grounding modification in the test setup allowed better detection of PD both by the antenna and the filter.

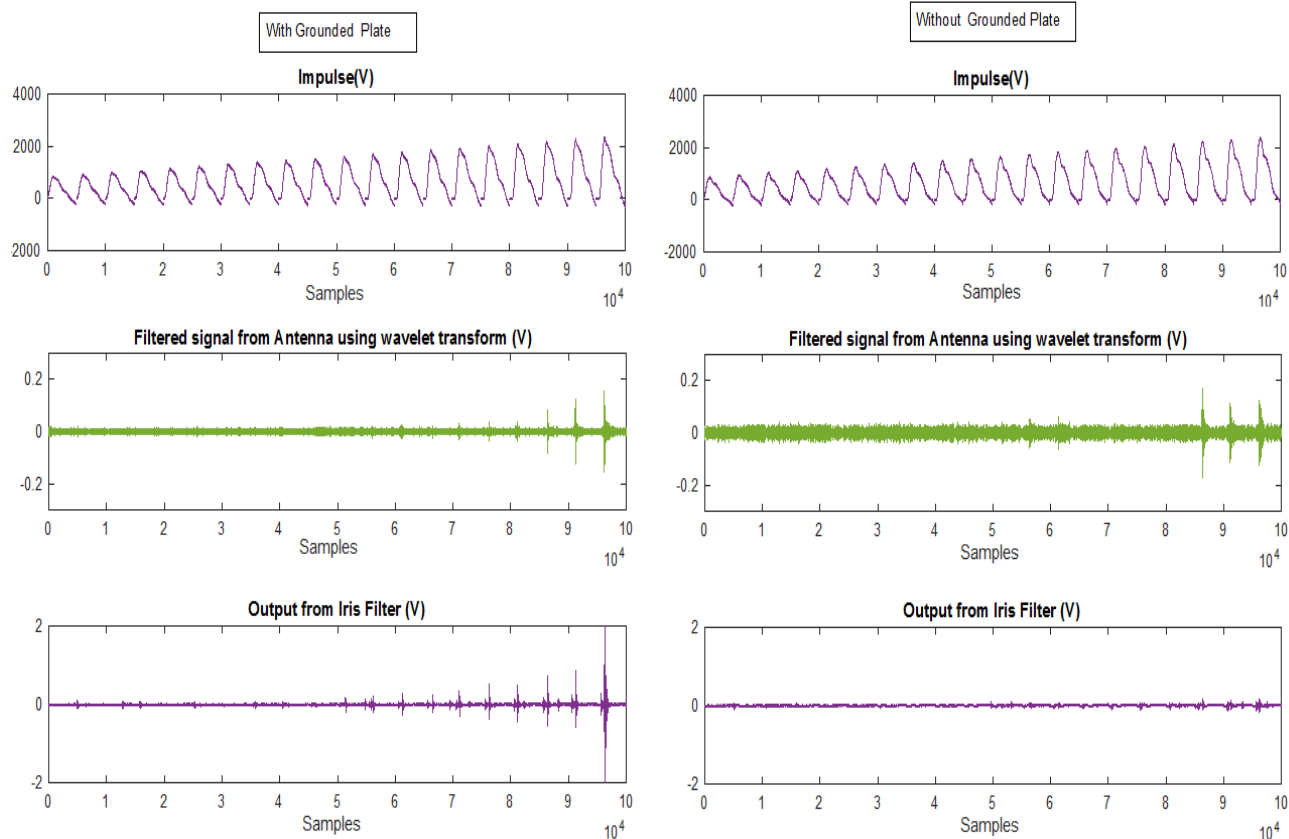


Figure 18: Comparison of PD detection in antenna and filter, with and without grounded steel plate for stator X26RA-175

Another important factor that was considered for PD detection was PD inception voltage (PDIV), as determined from both the filter and the antenna outputs. To determine PDIV, the lowest impulse voltage, which initiated a PD in antenna and filter, were recorded separately for both antenna and filter and then compared later. Results from ten successive PD tests conducted on stator X26RB-1_UV are shown in figure 18. Each trial represents an application of a train of impulse voltages, starting from a few hundred volts up to 3 to 3.5 KV with a frequency of 0.5 MHz.

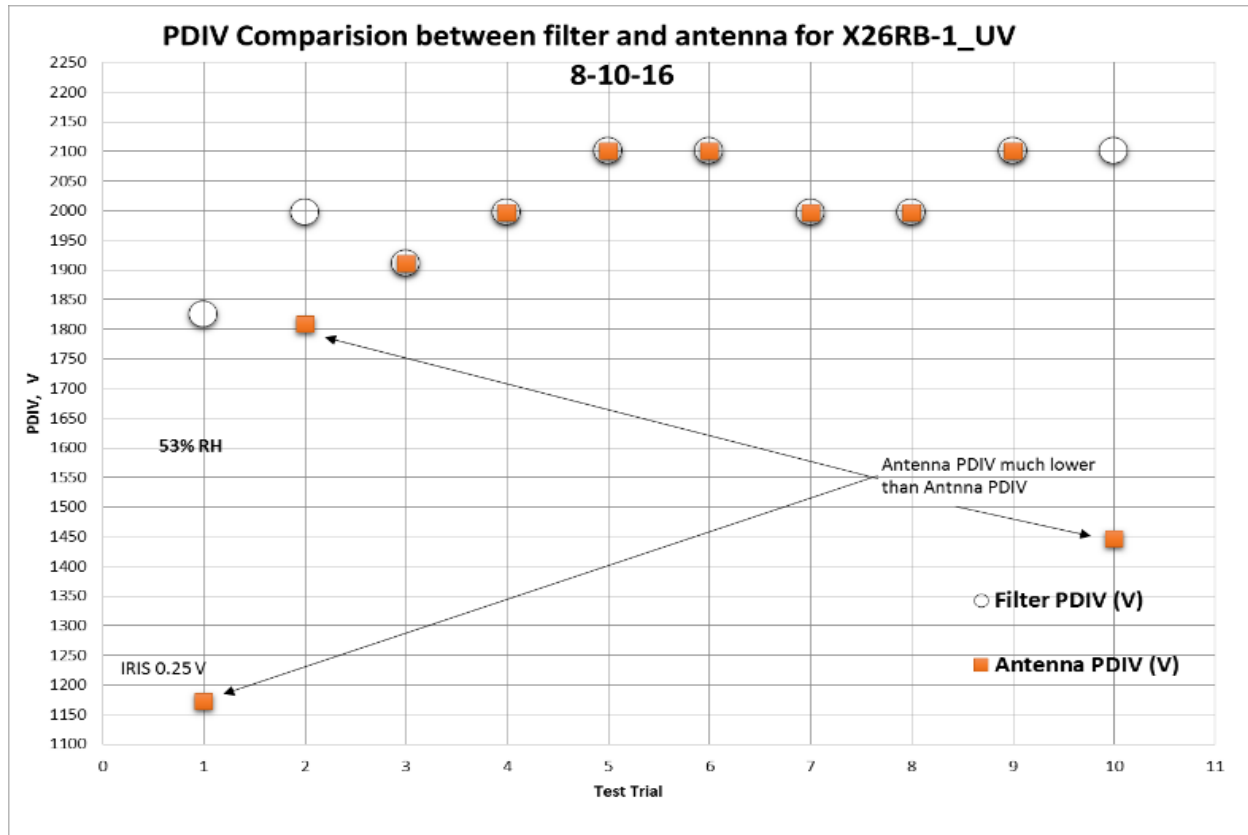


Figure 19: PD Inception voltages for stator X26RB-1 UV (10 trials)

Referring to figure 18, PDIV reported by antenna and filter for third through ninth trial were same. Whereas the PDIV reported for 1st, 2nd and 10th trial were different. Such cases of discrepancies between antenna and filter were inspected later for many other stators and trials to find the root cause. It was observed that first occurrence of PD in filter or antenna does not provide an accurate inception voltage for a stator because of the very first occurrence of PD questions the repeatability of occurrence of PD event.

In order to improve the PDIV decision made by the algorithm, each level of impulse voltage was applied six times to detect PD activity on a repetitive basis for every voltage level. To ensure high repeatability in detection, any particular voltage was considered as PDIV if it caused PD on at least three out of six times of its application on the stator. In this case, each test trial represents an

application of a train of impulse voltages, starting from a few hundred volts up to 3.0 to 3.5 KV, with a frequency of 0.5 MHz, with six repetitions of each voltage step.

As seen in figure 19, for this repetitive method, the filter and antenna show agreement on PDIV for all ten trials on the same stator X26RB. Hence, repetitions of PD event for any particular voltage level was considered to determine the PDIV for any stator under test.

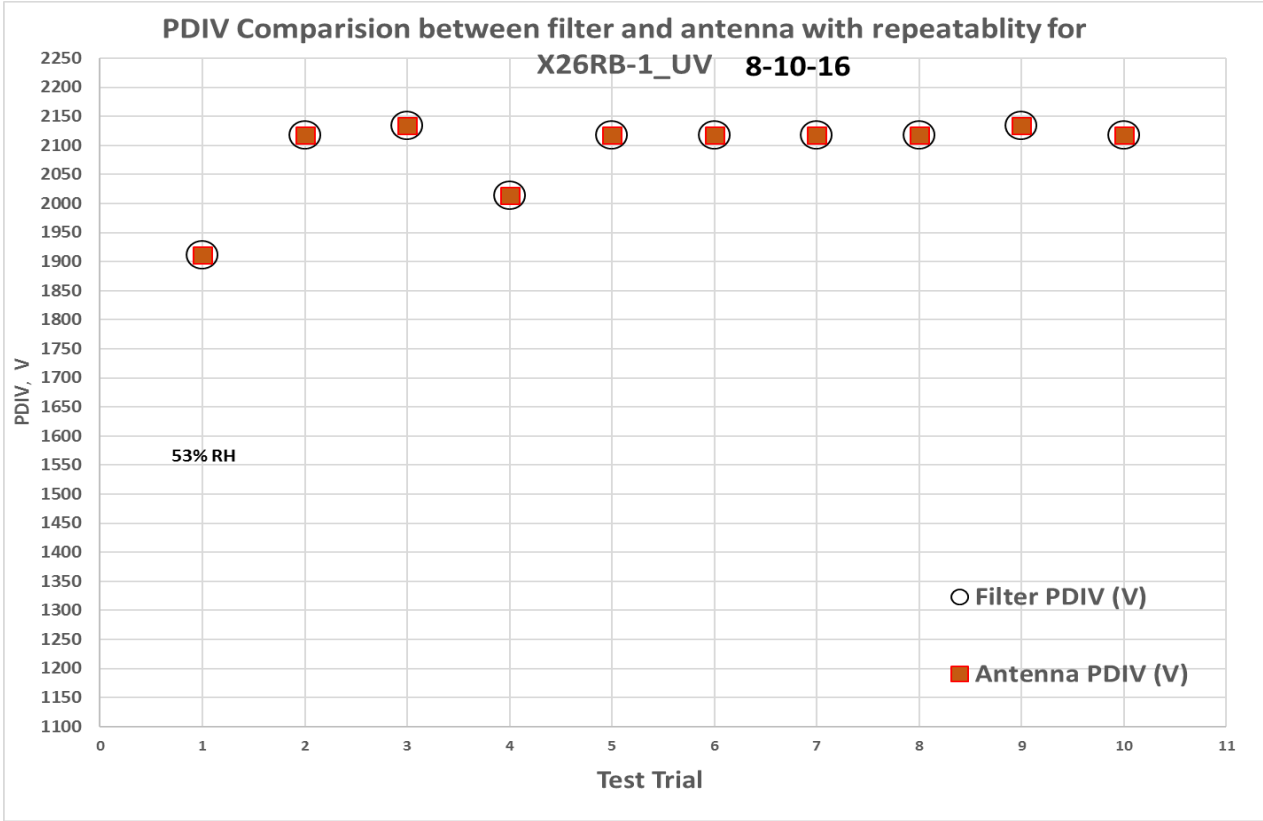


Figure 20: PD Inception voltages for stator X26RB-1_UV with repeatability

In order to see how the rejection of spurious noise signals improved the detection of PD in the antenna, comparison of consistency in PDIV reported by antenna before and after spurious noise rejection is presented in figure 21. The lowest value of impulse voltage, which initiated a detection, was recorded as PDIV for that particular trial. Figure 21 shows the results after DWT processing for 20 successive tests trials conducted on one stator, plotted in terms of PD inception voltages in order

to examine the consistency of the technique.

As seen from figure 21, after PD detection using the DWT output, most of the trials show the inception voltage to be around 2250 V. The irregularities similar to those observed in the 4th and 14th trials were due to the presence of spurious noise in the antenna as seen in Figure 13. Hence, DWT processing alone for extracting PD was not accurate enough to provide high consistency for recording the PD inception voltages.

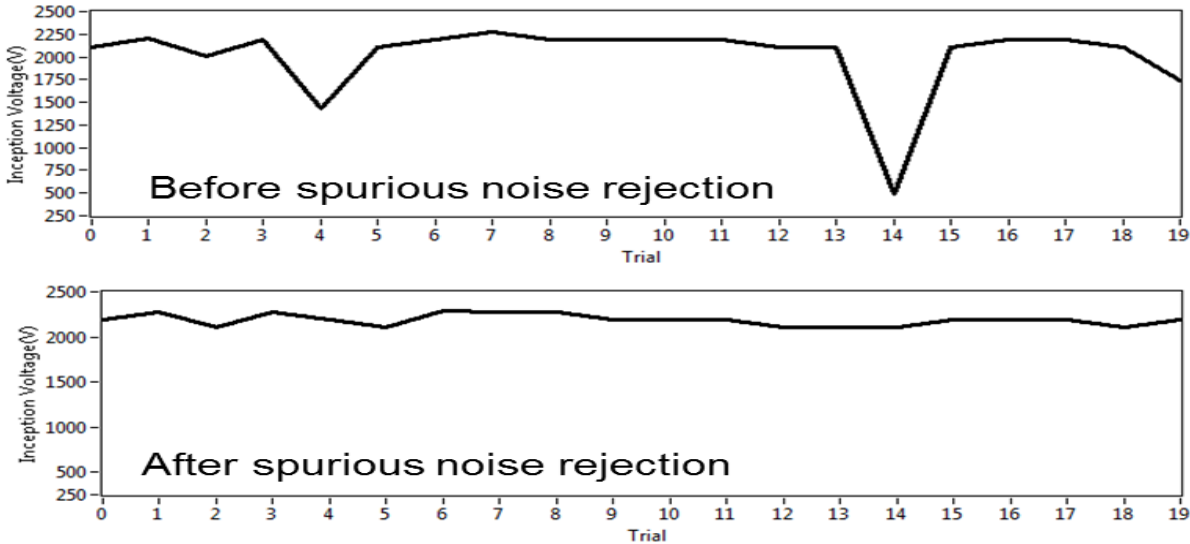


Figure 21: PD Inception voltages before and after eliminating noise by checking peak durations for stator X26RB-126 (20 trials)

In order to improve the PDIV decision using the antenna, the peak duration algorithm was applied after DWT processing of the antenna output, such that after threshold processing the PD signals extracted by the antenna, the duration of the peak was checked.

As seen in Figure 21, the cases of noise, which lowered the PDIV for trials 4 and 14 before applying peak duration criterion were eliminated (as explained in section 3.2.2). This made the PD detection scheme more consistent. It can be seen that the PDIV for this stator is around the mean of 2200 V. A similar trend is followed for similar comparisons for another stator in Figure 22.

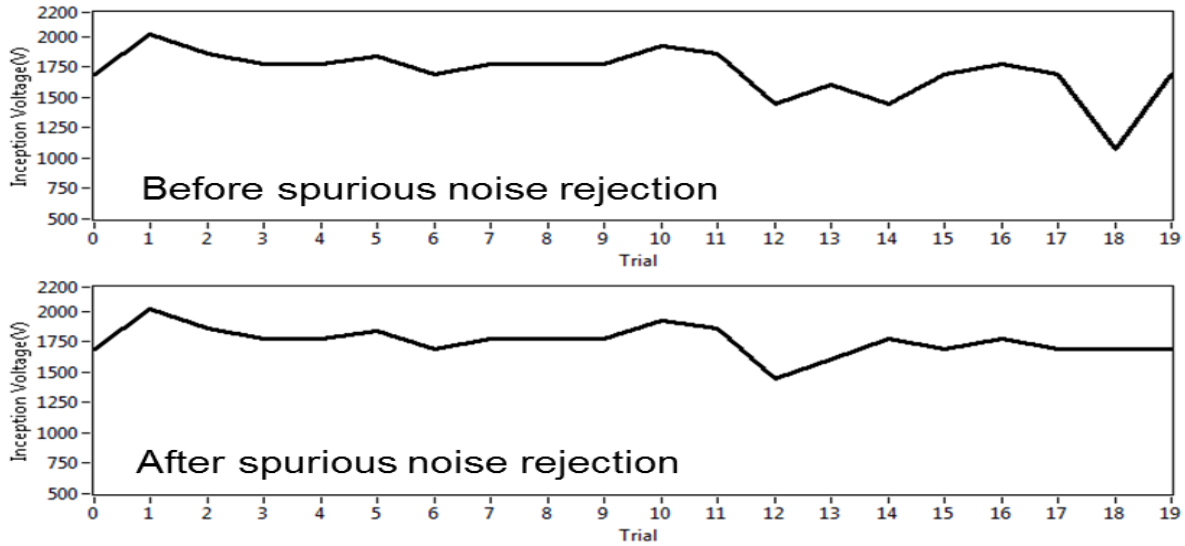


Figure 22: PD Inception voltages before and after eliminating noise by checking peak durations for stator X26RA-175 (20 trials).

Linear Discriminant Analysis (LDA) was used as another tool for antenna to provide better judgement of PD and noise events. As a first step, variables representing features of PD signal were selected, which can prove most effective to confirm the presence of PD.

In the process to perform accurate classification of PD, the following four features of the antenna (Db4 wavelet scale) were taken as input vectors:

- Peak to Peak value
- Signal to noise ratio
- Width of signal
- Integral within the region of peak

The values listed above were calculated to form four feature vectors consisting of 2141 samples, which included 312 samples of PD, 66 samples of spurious noise and 1763 samples of background noise. By using LDA as a dimension reduction technique (Section 2.3), the 4-D data was reduced to two dimensions, which allowed maximum separability of data into three classes as shown in figure 23.

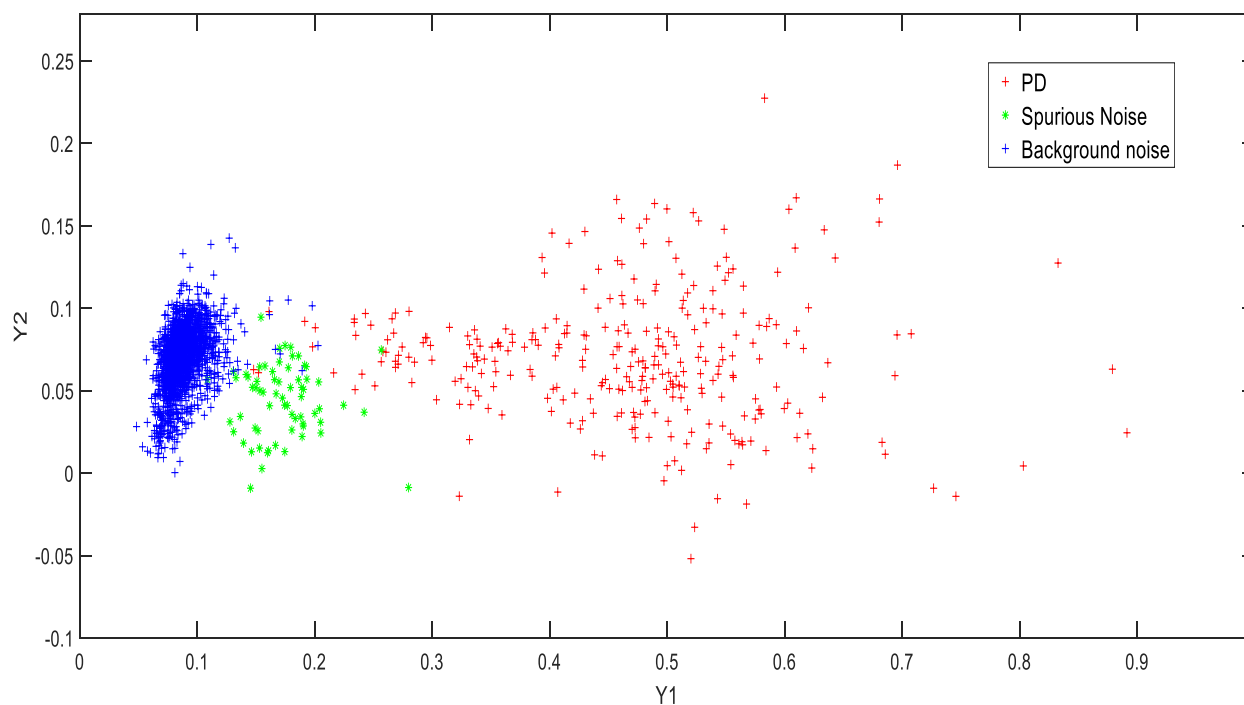


Figure 23: 2D representation of 4D sample dataset using LDA, showing maximum separability between classes.

The PD samples formed the most scattered group as seen by red spots in figure 23 whereas, spurious noise (green spots) and background noise (blue spots) are comparatively less scattered. Despite the fact that the three categories are not 100 percent separable, LDA provides a different method to classify the dataset.

It was interesting to see how linear discriminant functions would classify the sample dataset shown in figure 23 based on the algorithm discussed in section 2.3. Hence, classification training was performed using the same four features as used for the dimension reduction procedure.

The training did not converge even after 50000 iterations and implied that adjusted weights were unable to classify some samples correctly. The coefficients of the discriminant functions for three classes were obtained as follows, after adjusting the weighting coefficients 50000 times:

$\alpha_1 = [-2001.84 \quad 59.16161 \quad -62.9229 \quad 857.7974 \quad -19534]$
 $\alpha_2 = [\quad 968.759 \quad 74.66863 \quad 6146.289 \quad -1131.4 \quad 5152]$
 $\alpha_3 = [1033.508 \quad -127.824 \quad -5845.03 \quad 331.5564 \quad 14385]$

After close observation of results from LDA classification, results for the spurious noise category were found inaccurate. Therefore, the linear decision boundaries were ineffective to classify this type of data and may require nonlinear boundaries for its accurate classification.

VI. CONCLUSIONS AND FUTURE WORK

The PD detections made using the high-pass filter, with the antenna serving as a second reference, performed as a reliable detection technique for PD. The inception voltages for PD reported by this technique show considerable accuracy in detection after denoising is performed on both filter and antenna outputs. Results can be much better if the thresholds are optimized for both antenna and filter, depending on the type of stator to be used. The PD detection technique presented in this thesis provided a much better detection of PD events than techniques that use just one detection scheme, as it utilizes the benefits of both schemes. The correlation between outputs of filter and antenna can serve as an important tool to provide a reliable combined detection method.

The use of an antenna alone for PD detection showed good results especially after performing dimension reduction through LDA. The reduced dimensional data shows separability within the three classes. However, the classification of data using linear discriminant functions did not prove effective. Hence, the threshold process serves as a better and more efficient alternative, which calculates height and width of the pulse to declare it as PD or noise.

The separability of classes as seen from the LDA dimension reduction process may be utilized as part of future research. The other decision-making algorithms, especially non-linear discriminant functions, can be explored in future work to improve the classification of PD and noise cases.

APPENDIX

LabVIEW Programing steps

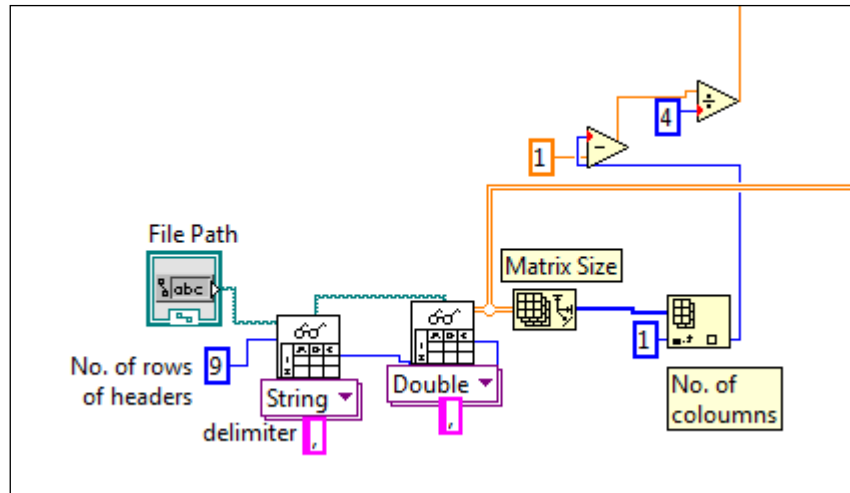


Figure 24: Programing blocks in LabVIEW which represent test data file (.csv) being read, rows of headers being separated and then matrix size is determined for setting the loop structures.

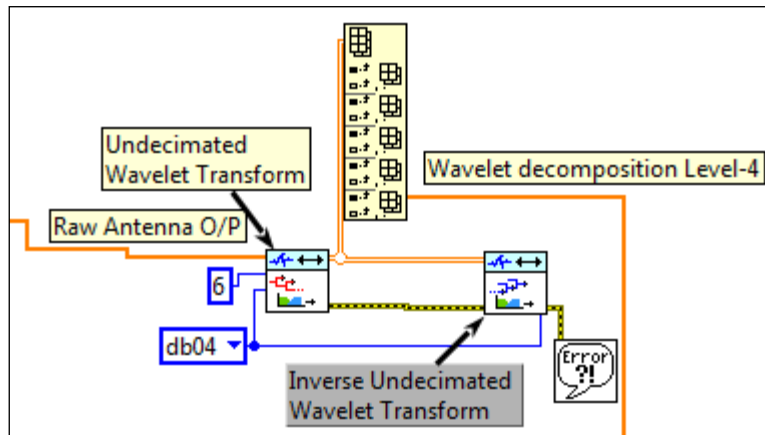


Figure 25: Process followed to decompose antenna signal by using “WA Undecimated Wavelet Transform VI” with settings of dB 6 and level 6. This provided wavelet decomposition level 4 scale which was used to detect PD events by the antenna.

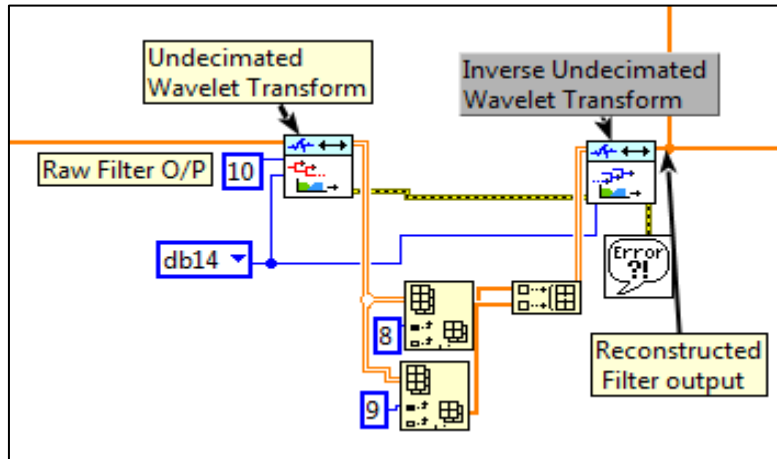


Figure 26: Process followed to decompose filter signal by using “WA Undecimated Wavelet Transform VI” with settings of dB 14 and level 10. Levels 8 and 9 were selected for reconstruction through “WA Inverse Undecimated Wavelet Transform VI”. This provided reconstructed filter output, which was used to detect PD events by the filter.

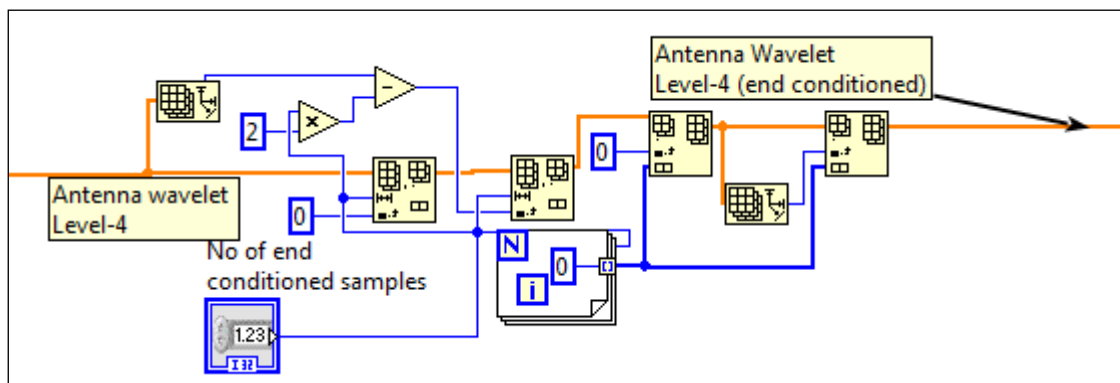


Figure 27: The values at the first and last 25 samples of denoised antenna output were set to zero to treat the end-condition problem in antenna waveform.

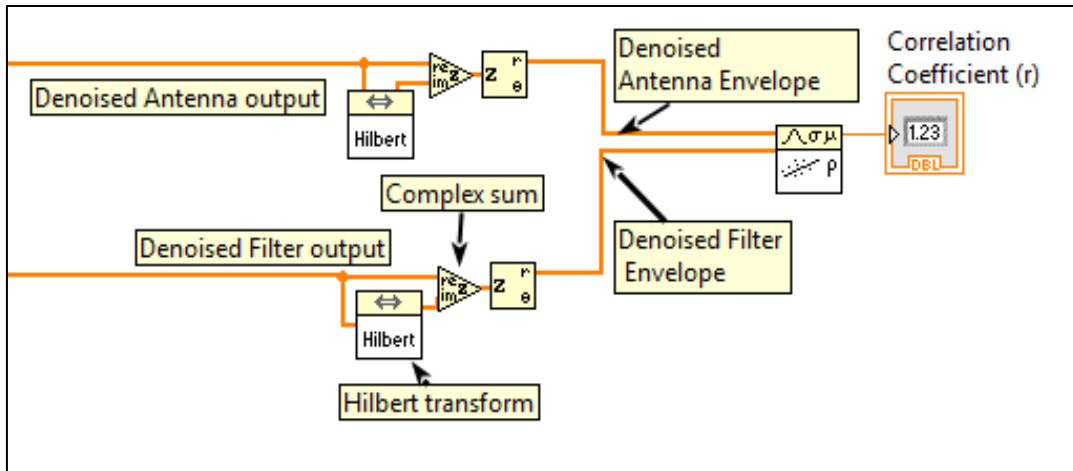


Figure 28: Envelopes of the denoised antenna and filter outputs are found and then cross-correlation coefficient is calculated using both to reflect similarity between the two signals.

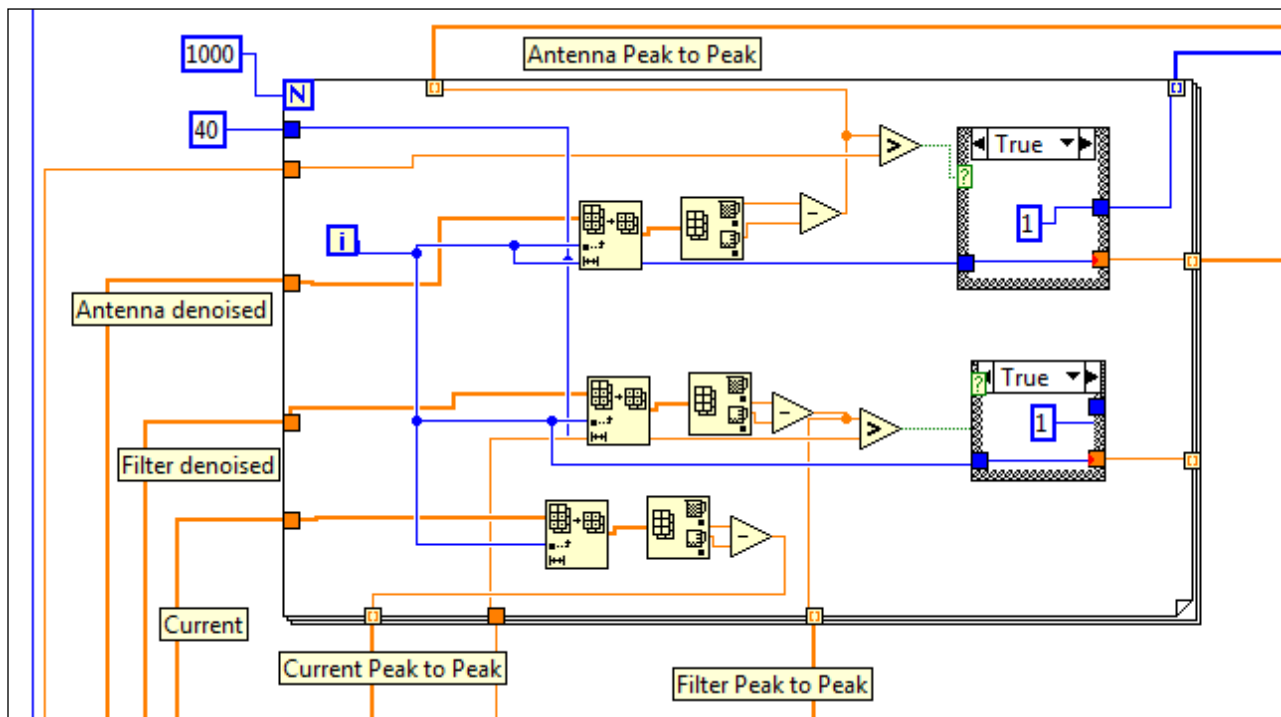


Figure 29: Peak to Peak values at each sample is calculated for current, denoised antenna and filter output by considering a window of 40 samples.

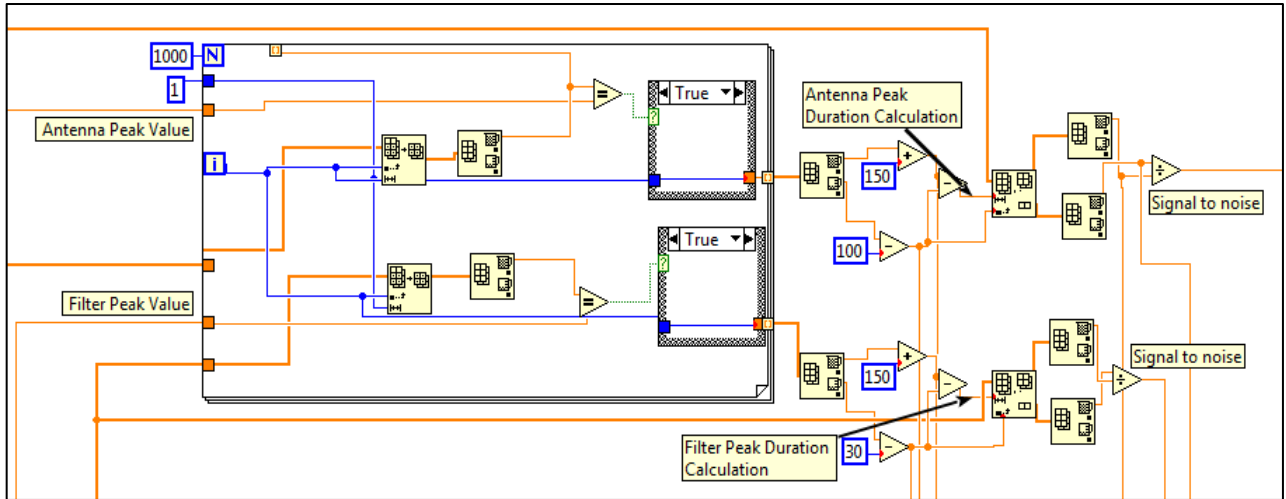


Figure 30: Peak values of the denoised antenna and filter output are compared with signals themselves to find the regions of peak and then signals to noise ratio is determined for the two signals based on these regions of the peak (PD) and noise (no PD).

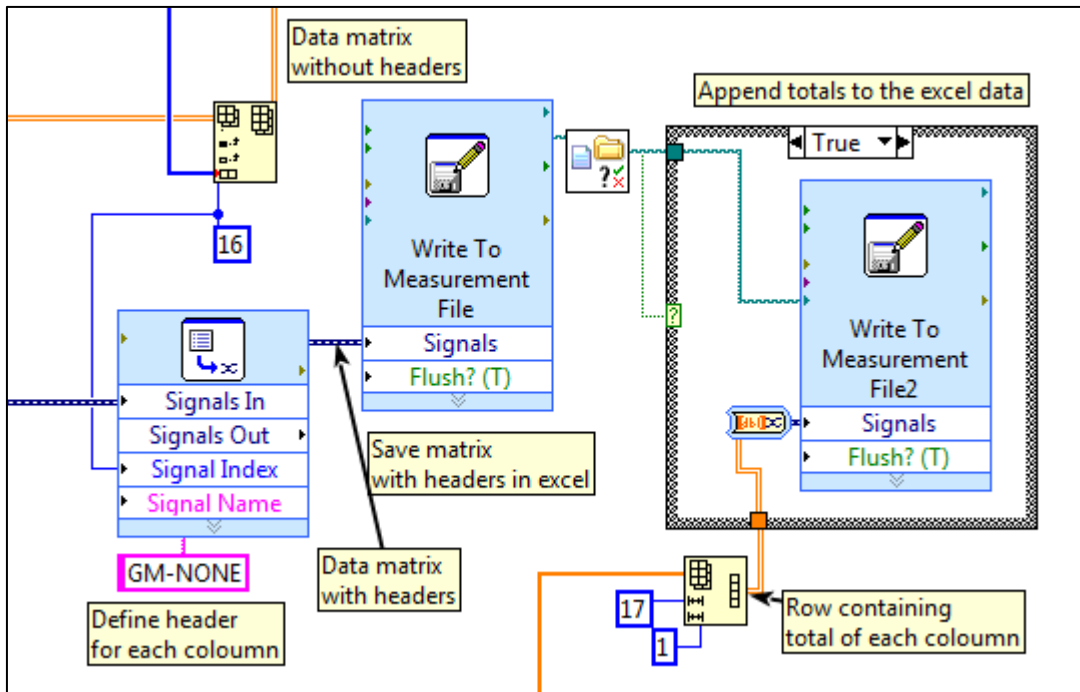


Figure 31: All the variables calculated within the program for each level of applied impulse voltage are written along with headers to an excel spreadsheet named and located by the user.

Laboratory Setup

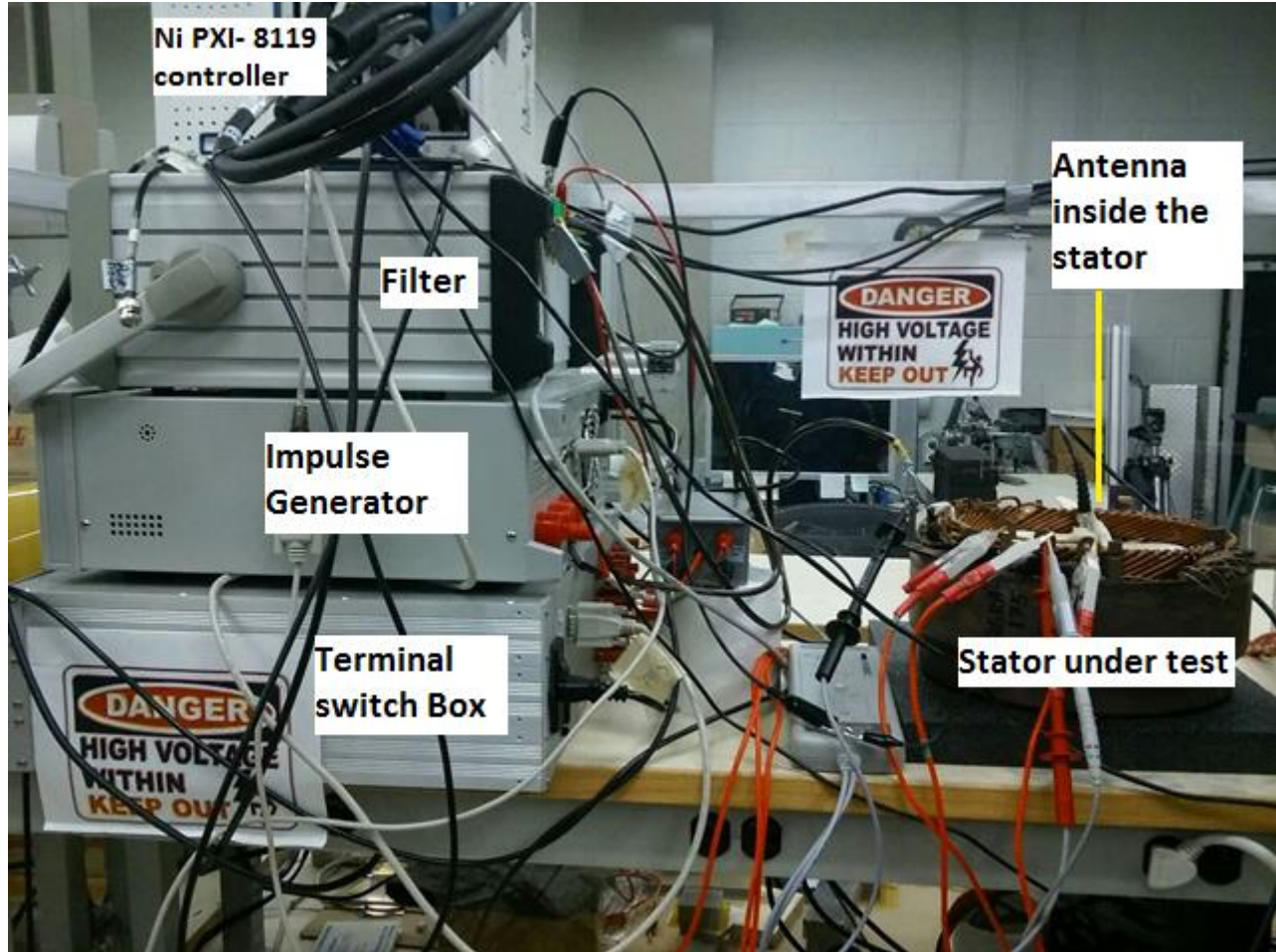


Figure 32: Picture of the experimental setup used for PD test without grounded steel plate.

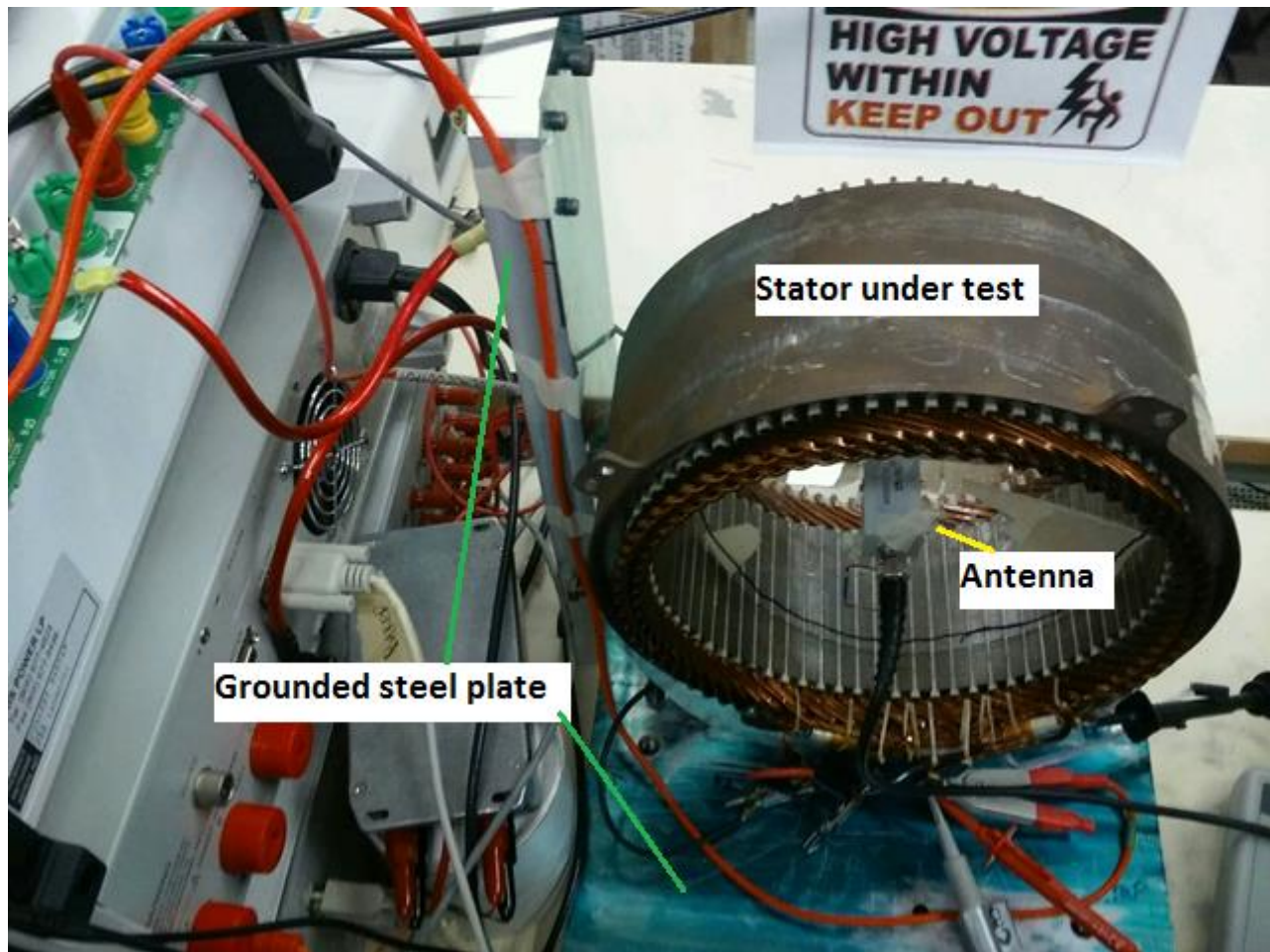


Figure 33: Top view of Experimental setup showing connections made using grounded steel plate using an antenna.

REFERENCES

REFERENCES

- [1] G. Paoletti, A. Golubev, "Partial discharge theory and applications to electrical systems," Conference Record of 1999 Annual Pulp and Paper Industry Technical Conference (Cat. No.99CH36338), 1999, pp. 124-138.
- [2] G. C. Stone, E. A. Boulter, I. Culbert, and H. Dhirani, "Electrical insulation for rotating machines - design, evaluation, aging, testing, and repair". IEEE Press, John Wiley and Sons, Volume: 20, Issue: 3, 2004, pp. 65 – 65.
- [3] F. Guastavino, E. Torello, M. Di Lorenzo del Casale, L. Egiziano: "Voltage distortion effects on insulation systems behavior in ASD motors", 2003 Annual Report Conference on Electrical Insulation and Dielectric Phenomena, 2003, pp. 608-611.
- [4] H. Okubo, et al., "Technical development on partial discharge measurement and electrical insulation techniques for low voltage motors driven by voltage inverters" IEEE Transactions on Dielectrics and Electrical Insulation, Vol. 14, No. 6, 2007, pp.1516-1530.
- [5] G. Stone, S. Campbell, and S. Tetreault, "Inverter-fed drives: which motor stators are at risk?" IEEE Industry Applications Magazine, vol. 6, no. 5, Sep/Oct 2000, pp. 17-22.
- [6] G. C. Stone, "Partial discharge diagnostics and electrical equipment insulation condition assessment," IEEE Transactions on Dielectrics and Electrical Insulation, vol. 12, no. 5, Oct. 2005, pp. 891-904.
- [7] Prabhakar Neti and Stefan Grubic, "Online broadband insulation spectroscopy of induction machines using signal injection," IEEE Transactions on Dielectrics and Electrical Insulation, 2014 IEEE Energy Conversion Congress and Exposition (ECCE), Pittsburgh, PA, 2014, pp. 630-637.
- [8] Jinkyu Yang, Tae-June Kang, Byunghwan Kim, and Sang Bin Lee, "Experimental evaluation of using the surge pd test as a predictive maintenance tool for monitoring turn insulation quality in random wound ac motor stator windings," IEEE Transactions on Dielectrics and Electrical Insulation, vol. 19, no. 1, February 2012, pp. 53-60.
- [9] R. Bartnikas, "Partial discharges. their mechanism, detection, and measurement", IEEE Transactions on Dielectrics and Electrical Insulation, vol. 9, no. 5, Oct 2002, pp. 763-808.
- [10] Yong-Joo Kim, Dong-Sik Kang, Don-Ha Hwang, Ioan Haiduc, "Factory measurement system for sub pico coulomb partial discharge signal," Electrical Insulation Conference and Electrical Manufacturing and Coil Winding Technology Conference (Cat. No.03CH37480), 2003, pp. 347-351.
- [11] G.C. Stone, V. Warren, "Advancements in interpreting partial discharge test results to assess stator winding condition," IEEE-IAS/PCA 2004 Cement Industry Technical Conference (IEEE Cat. No04CH37518), 2004, pp. 61-65.

- [12] IEEE guide to the measurement of partial discharges in rotating machinery, IEEE Std 1434-2000, Aug. 15 2000, pp.1-64.
- [13] G. C. Stone and V. Warren, "Advancements in interpreting partial discharge test results to assess stator winding condition," IEEE-IAS/PCA 2004 Cement Industry Technical Conference (IEEE Cat. No04CH37518), 2004, pp. 61-65.
- [14] B. Sarkar, D. K. Mishra, C. Koley and N. K. Roy, "Microstrip patch antenna based UHF sensor for detection of Partial Discharge in High Voltage electrical equipments," 2014 Annual IEEE India Conference (INDICON), Pune, 2014, pp. 1-6.
- [15] L. Angrisani, M. Di Lorenzo del Casale, M. D'Arco and C. Petrarca, "Extraction of PD data from UWB measurements on motor stator bars fed by an IGBT inverter," Annual Report Conference on Electrical Insulation and Dielectric Phenomena, 2002, pp. 844-847.
- [16] Duan Dapeng; Teng Letian; Qian Yong; Wang Jiang; Huang Chengjun; Zeng Yi; Jiang Xiuchen, "Experimental study and feature extraction on UHF partial discharge detection for typical model in air," 2008 International Conference on Condition Monitoring and Diagnosis, Beijing, 2008, pp. 1040-1043.
- [17] Jian Li; Tianyan Jiang; Robert F. Harrison; Stanislaw Grzybowski, "Recognition of ultra high frequency partial discharge signals using multi-scale features," IEEE Transactions on Dielectrics and Electrical Insulation, Volume: 19, Issue: 4, August 2012, pp.1412 - 1420
- [18] G. Robles, M. Sánchez-Fernández, R. Albarracín Sánchez, M. V. Rojas-Moreno, E. Rajo-Iglesias and J. M. Martínez-Tarifa, "Antenna Parametrization for the Detection of Partial Discharges," in IEEE Transactions on Instrumentation and Measurement, vol. 62, no. 5, pp. 932-941, May 2013.
- [19] T. Jiang, J. Li, M. Chen and S. Grzybowski, "Recognition on ultra-high-frequency signals of partial discharge by support vector machine," 2010 International Conference on High Voltage Engineering and Application, New Orleans, LA, 2010, pp. 634-637.
- [20] H. B. Khamseh, V. S. P. Ruela, F. H. Vasconcelos and H. d. O. Mota, "Mining undecimated Wavelet Transform maxima lines: An effective way to denoise partial discharge signals," 2014 IEEE Electrical Insulation Conference (EIC), Philadelphia, PA, 2014, pp. 260-266.
- [21] P. K. Shetty and T. S. Ramu, "An undecimated wavelet transform based denoising, PPCA based pulse modeling and detection-classification of PD signals," Proceedings of the 17th International Conference on Pattern Recognition, 2004. ICPR 2004., 2004, pp. 873-876 Vol.4.
- [22] S. Mallat, A Wavelet Tour of Signal Processing, 3rd edition. Burlington Academic Press, 2009.
- [23] T. Y. Young and T. W. Calvert, "Classification, Estimation And Pattern Recognition", American Elsevier Publishing Co., Inc., 1974.

[24] Claerbout, Jon F. *Fundamentals of Geophysical Data Processing with Applications to Petroleum Prospecting*. Oxford, UK: Blackwell, 1985, pp. 59–62.

[24] Marple, S. L. "Computing the Discrete-Time Analytic Signal via FFT." *IEEE Transactions on Signal Processing*, Vol. 47, 1999, pp. 2600–2603.

[25] Oppenheim, Alan V., Ronald W. Schaffer, and John R. Buck, "Discrete-Time Signal Processing", 2nd Ed. Upper Saddle River, NJ: Prentice Hall, 1999.

[26] D. S. Laila, M. Larsson, B. C. Pal and P. Korba, "Nonlinear damping computation and envelope detection using Hilbert transform and its application to power systems wide area monitoring," 2009 IEEE Power & Energy Society General Meeting, Calgary, AB, 2009, pp. 1-7.